



Design, synthesis and molecular docking of new fused 1*H*-pyrroles, pyrrolo[3,2-*d*]pyrimidines and pyrrolo[3,2-*e*][1, 4]diazepine derivatives as potent EGFR/CDK2 inhibitors

Amany Belal^{a,b} , Nagwa M. Abdel Gawad^c, Ahmed B. M. Mehany^d, Mohammed A. S. Abourehab^{e,f}, Hazem Elkady^g, Ahmed A. Al-Karmalawy^h  and Ahmed S. Ismael^a

^aMedicinal Chemistry Department, Faculty of Pharmacy, Beni-Suef University, Beni-Suef, Egypt; ^bDepartment of Pharmaceutical Chemistry, College of Pharmacy, Taif University, Taif, Saudi Arabia; ^cMedicinal Chemistry Department, Faculty of Pharmacy, Cairo University, Giza, Egypt; ^dDepartment of Zoology, Faculty of Science, Al-Azhar University, Nasr City, Egypt; ^eDepartment of Pharmaceutics, Faculty of Pharmacy, Umm Al-Qura University, Makkah, Saudi Arabia; ^fDepartment of Pharmaceutics and Industrial Pharmacy, College of Pharmacy, Minia University, Minia, Egypt; ^gPharmaceutical Medicinal Chemistry & Drug Design Department, Faculty of Pharmacy (Boys), Al-Azhar University, Cairo, Egypt; ^hDepartment of Pharmaceutical Medicinal Chemistry, Faculty of Pharmacy, Horus University- Egypt, New Damietta, Egypt

ABSTRACT

A new series of 1*H*-pyrrole (**6a–c**, **8a–c**), pyrrolo[3,2-*d*]pyrimidines (**9a–c**) and pyrrolo[3,2-*e*][1, 4]diazepines (**11a–c**) were designed and synthesised. These compounds were designed to have the essential pharmacophoric features of EGFR Inhibitors, they have shown anticancer activities against HCT116, MCF-7 and Hep3B cancer cells with IC₅₀ values ranging from 0.009 to 2.195 μM. IC₅₀ value of doxorubicin is 0.008 μM, compounds **9a** and **9c** showed IC₅₀ values of 0.011 and 0.009 μM respectively against HCT-116 cells. Compound **8b** exerted broad-spectrum activity against all tested cell lines with an IC₅₀ value less than 0.05 μM. Compound **8b** was evaluated against a panel of kinases. This compound potently inhibited CDK2/Cyclin A1, DYRK3 and GSK3 alpha kinases with 10–23% compared to imatinib (1–10%). It has also arrested the cell cycle of MCF-7 cells at the S phase. Its antiproliferative activity was further augmented by molecular docking into the active sites of EGFR and CDK2 cyclin A1.

ARTICLE HISTORY

Received 20 April 2022
Revised 23 June 2022
Accepted 26 June 2022

KEYWORDS

Anticancer; 1*H*-pyrrole; pyrrolo[3,2-*d*]pyrimidine; pyrrolo[3,2-*e*][1, 4]diazepine; EGFR inhibitor; CDK2 inhibitor






1. Introduction


Cancer is clearly associated with an increased incidence and rates of mortality, in addition to its devastating social and economic effects^{1,2}. Cancer is a generic term for a large group of diseases that can affect any part of the human body^{2,3}. The complexity of cancer pathologies manifests in oncogenic mutations, severe and occasionally fatal drug side effects, multi-drug resistance and activation of compensatory pathways^{4–6}. Thus, there is an urgent need to develop more efficient anticancer candidates, relying on various biological and molecular aspects of neoplastic transformation. Accordingly, many efforts were done to reach promising anticancer candidates^{1,7–10}.

Protein kinases constitute one of the largest and most functionally diverse gene families that control a diverse set of cellular processes. Thus, they perform a major role in the proliferation, metastasis and survival of human tumour cells¹¹. Tyrosine kinase is the most important protein kinases sub-family. This family comprises epidermal growth factor receptor (EGFR)¹², vascular endothelial growth factor receptor (VEGFR)¹³, fibroblast growth factor receptor (FGFR)¹⁴ and cyclin-dependent kinases (CDK)¹⁵. Three of the protein kinases have been crystallised in active conformations (cAPK, PhK, and CK1), one in a partially active conformation (CDK2

in complex with cyclin A), and five in inactive conformations (CDK2, MAPK, IRK, twitchin kinase, and CaMKI). The structures of the kinases in the active conformation all showed equivalent positions for essential catalytic site residues Lys-72, Asp-166, and Asp-184 in cAPK. Their positions and the correct orientation of the Mg²⁺/ATP and the protein substrate appear crucial for catalysis and are dependent upon the tertiary structure of both lobes and the correct relative orientation of the lobes. In the partially active CDK2–cyclin A complex, the charge grouping is compensated by glutamate, Glu-162, (two residues removed from the phosphorylatable threonine Thr-160) and by interactions of arginyl residues with the main chain carbonyl groups from cyclin A. In PhK, there is only one basic group, the arginine adjacent to the catalytic base, and charge compensation can be satisfactorily accomplished by a carboxylate group¹⁶.

The epidermal growth factor receptor (EGFR) is a transmembrane protein receptor endowed with tyrosine kinase activity, occupying an important position in cancer progression and tumour cell biology. EGFR plays a role in cellular phenotyping and provides tumour cells with significant growth¹⁷. Elevated levels of EGFR and its associated ligands (EGF and transforming growth factor (TGF)) have been found to be a common feature of a variety of cancer types. In many cases, abnormal EGFR activation appears

CONTACT Amany Belal  abilalmoh1@yahoo.com; amany.mehani@pharm.bsu.edu.eg; Ahmed S. Ismael  ahmed_safwat1987@yahoo.com, ahmed.safwat@pharm.bsu.edu.eg  Medicinal Chemistry Department, Faculty of Pharmacy, Beni-Suef University, Beni-Suef, 62514, Egypt; Nagwa M. Abdel Gawad  nagwa_gawad2010@yahoo.com  Medicinal Chemistry Department, Faculty of Pharmacy, Cairo University, Kasr El-Eini Street 11562, Egypt

 Supplemental data for this article is available online at <https://doi.org/10.1080/14756366.2022.2096019>.

© 2022 The Author(s). Published by Informa UK Limited, trading as Taylor & Francis Group.

This is an Open Access article distributed under the terms of the Creative Commons Attribution License (<http://creativecommons.org/licenses/by/4.0/>), which permits unrestricted use, distribution, and reproduction in any medium, provided the original work is properly cited.

to be a key element in carcinogenesis and a major driving force for cancer growth¹⁸. Increased EGFR expression is thus expected to be a powerful prognostic factor in a variety of tumour forms and blocking its cellular functions looks to have significant therapeutic effects¹⁹. As a result, EGFR is being regarded as a viable target for the development of novel anticancer drugs^{20–23}.

The cyclin-dependent kinases (CDKs) are a group of enzymes involved in cell cycle progression and cellular proliferation²⁴. They work by phosphorylating critical serine and threonine residues in host proteins, which then can activate them^{25,26}. It is commonly believed that inhibiting CDKs could help the limitation of the uncontrolled cellular proliferation seen in some malignancies²⁷. The majority of CDK inhibitors bind to the ATP pocket as ATP-competitive inhibitors with essential structural hydrogen-bonding motifs²⁸. Cyclin-dependent kinase 2 (CDK2) belongs to the serine/threonine protein kinase family, and the CDK2 activity is found to be typically high in different types of human cancers. Studies have reported that CDK2 overexpression indicates poor prognosis in patients with HCC, and inhibition of CDK2 activity could reverse the malignant phenotype of cancer cells. Many studies revealed a key role of CDK2 in EGF-induced cell transformation and the associated signal transduction pathways²⁹. The literature survey revealed that EGFR and CDK2 were the key targets for many anti-tumor agents e.g. cinobufagin³⁰. In addition, biological and computational evidence supported that anticancer agents such as benzamide-substituted chalcones exerted their anti-proliferative effects via dual EGFR/CDK2 inhibitory activities³¹.

It is worth mentioning that, dual-specificity tyrosine phosphorylation-regulated kinase 3 (DYRK3) is a regulator of phase transition during mitosis³². Furthermore, it is able to promote mTORC1 activity, which is associated with resistance to EGFR-mediated endocrine therapy, and other forms of targeted therapy, also it regulates fundamental cellular functions including transcription, translation, proliferation, growth and survival³³. Moreover, Glycogen synthase kinase 3 (GSK3) is involved in modulating numerous signalling pathways affecting metabolism, tumorigenesis, proliferation, apoptosis, autophagy, development, and differentiation involved in metabolic regulation³⁴. GSK3 inhibitors were reported to suppress breast tumour growth in pre-clinical models^{35,36}.

Until now, there are many FDA-approved drugs for the treatment of cancer targeting EGFR as erlotinib **I** and afatinib **II**. The first generation of these inhibitors (as erlotinib **I**) gave good benefits in the treatment of non-small-cell lung cancer³⁷. The second generation of EGFR inhibitors (as afatinib **II**) was approved to overcome EGFR mutation-related resistance³⁸. The third generation of EGFR inhibitors (as rociletinib **III**) had overcome induced toxicity caused by 2nd generation^{39–41}. Palbociclib **IV** is the first FDA-approved cyclin-dependent kinase inhibitor that acts by binding to the ATP pocket with an IC₅₀ in the range of 9–15 nM²⁷ (Figure 1).

EGFR inhibitors have some pharmacophoric features which are essential for maximal affinity against the ATP binding site of EGFR. These features include i) a flat hetero aromatic ring system that occupies the adenine binding pocket⁴², ii) terminal hydrophobic head which can occupy the hydrophobic region I, iii) imino group (NH, spacer) which can occupy the space between the adenine binding region and the hydrophobic region I⁴³, iv) hydrophobic tail which occupies the hydrophobic region II^{44,45}, ribose binding moiety which can occupy the ribose binding pocket. Till now, there are limitations in research that target the ribose binding pocket⁴⁶ (Figure 2).

Privileged structures of diazepine have been widely used as effective templates for anticancer agents especially targeting EGFR enzyme⁵⁰. Xu et al., described in 2013 a compound with a 1,3-diazepine moiety (compound **V**) presenting a potent inhibition activity against the EGFR790M mutant (IC₅₀ = 3.36 nM) and the double EGFR L858R/T790M mutant (IC₅₀ = 1.69 nM)⁵¹. Also, in 2019, a series of thieno[2,3-*d*]pyrimidine derivatives were designed and synthesised as EGFR and HER2 tyrosine kinase inhibitors. Compound **VI** exhibited promising cytotoxic activity⁴⁷. In 2020, a new series of pyrimidine-5-carbonitrile derivatives were designed and synthesised as EGFR inhibitors. Compound **VII** showed high inhibitory activities against EGFR^{WT} and EGFR^{T790M48} (Figure 1).

Based on the mentioned facts and as an extension of the previous efforts in the design and synthesis of new anticancer agents^{48,52–59} especially to target EGFR^{47,48,60} we used the 1*H*-pyrrole, pyrrolo[3,2-*d*]pyrimidine, and pyrrolo[3,2-*e*][1, 4]diazepine moieties as building blocks for the design and synthesis of new EGFR and CDK inhibitors (Figure 3).

1.1. Rationale of molecular design

In the present work, the previously active compounds (**V**, **VI** and **VII**) were used as lead compounds to design new EGFR inhibitors. Dramatic modifications were achieved to reach more promising active candidates against EGFR and CDK. The modifications were performed on four features. The flat hetero aromatic system was modified to be 1*H*-pyrrole (compounds **6a–c** and **8a–c**) (Scaffold **A**), pyrrolo[3,2-*d*]pyrimidine (**9a–c**) (Scaffold **B**), and pyrrolo[3,2-*e*][1, 4]diazepine (compounds **11a–c**) (Scaffold **C**). ii) For the terminal hydrophobic head, we used different hydrophobic moieties as substituted phenyl groups (compounds **6a–c**) or aliphatic moieties (compounds **8a–c**, **9a–c**, and **11a–c**). Regarding the hydrophobic tail, we used the pyrrolidine moiety in all the designed compounds. The NH spacer was kept as it is in compounds **8a–c**, whereas it was changed into -N= moiety in compounds **6a–c**, and deleted in compounds **9a–c** relating on the two nitrogen atoms of pyrimidine moiety to act as hydrogen bond centres. Moreover, in compounds **11a–c**, it was modified to be inside the ring structure as a heteroatom. To occupy ribose binding moieties, we used different aromatic structures. Different structure modifications were then achieved to obtain a SAR study as a second aim in our work.

To confirm our rationale, the synthesised compounds were investigated for their antiproliferative activities against a panel of human cancer cell lines (Hep3B, HCT116, and MCF-7). In addition, the most active anti-proliferative agent was further subjected to a Kinase profiling test to assess its activity against EGFR, CDK, and other kinases. Furthermore, to reach a good insight into the activity of the most active candidate at the molecular level, cell cycle analysis was carried out. Finally, *in silico*, docking, ADMET, and toxicity studies were performed to predict the possible binding interaction of the synthesised compounds against the prospective targets (EGFR and CDK) as well as to calculate the proposed kinetic and toxicity profile.

2. Results and discussion

2.1. Chemistry

Compounds **8**⁶¹ and **10a–c**⁶² were synthesised according to reported methods, which were then used to afford the intermediates **11a–c** according to the reported procedure⁶³. Condensation of compounds **5a–c** (Scheme 1) with 4-nitrobenzaldehyde in

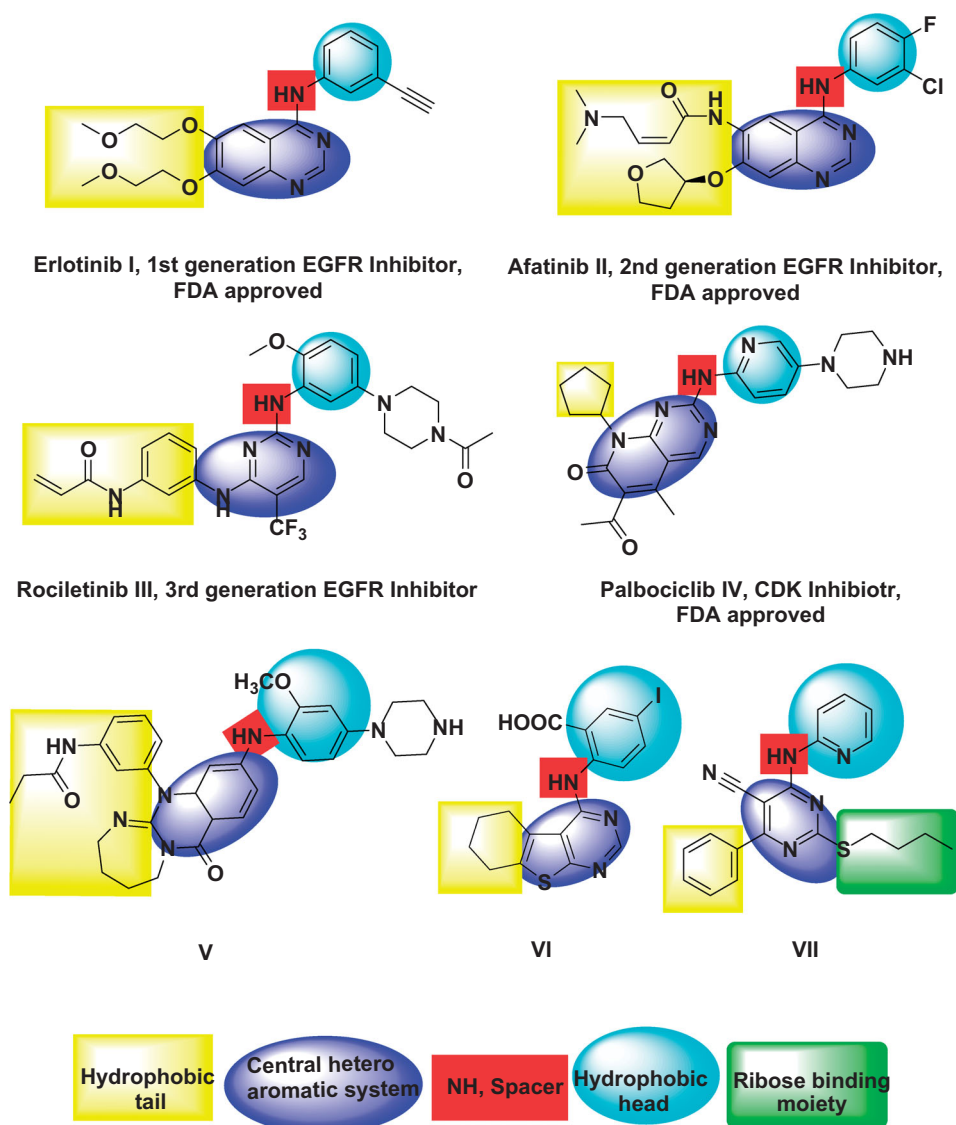


Figure 1. FDA approved and reported kinases inhibitors with their essential pharmacophoric features.

absolute ethanol afforded three Schiff base derivatives (**6a–c**, Scheme 2). The IR spectra of compounds **6a–c** showed sharp absorption bands at $2210\text{--}2214\text{ cm}^{-1}$, indicating the cyano group. Furthermore, the ^1H NMR spectra of compounds **6a–c** showed two doublet signals at a range of 8.10–8.42 ppm due to the aromatic protons of the 4-nitrobenzylidene moiety. Moreover, a singlet signal appeared at a range of 9.28–9.31 corresponding to the $\text{N}=\text{CH}$ proton. While their ^{13}C NMR spectra revealed two signals at a range of 156.3–158 ppm indicating the $\text{N}=\text{CH}$ and the carbonyl carbon in each of the three derivatives. The free amino group of compounds **5a–c** was further acylated with 2-chloroacetyl chloride to give compounds **7a–c**. Compounds **8a–c** were prepared by *N*-alkylation of piperidine with the terminal chlorinated side chain of **7a–c** in absolute ethanol, using sodium bicarbonate to neutralise the hydrogen chloride liberated from this reaction (Scheme 2). The ^1H NMR spectra of compounds **7a–c** confirmed the aliphatic protons of the piperidin-1-yl ring; multiplet and triplet signals at a range of 1.50–2.74 ppm. Their ^{13}C NMR spectra further revealed three additional signals in the range of 23.4–55.0 ppm due to the aliphatic carbons of the piperidin-1-yl ring.

Moreover, several studies reported the use of triethyl orthoformate to produce cyclized derivatives⁶⁴. The tricyclic pyrrolo[3,2-*d*]pyrimidine derivatives **9a–c** were achieved by refluxing compounds **5a–c** with excess triethyl orthoformate (Scheme 3). The NHs stretching bands disappeared in the IR spectra of compounds **9a–c**. Further, the ^1H NMR spectra of compounds **9a–c** confirmed disappearance of the exchangeable protons' signals, corresponding to compounds **5a–c** NHs protons. Additionally, they showed singlet signals at a range of 2.25–2.27 ppm corresponding to the aliphatic methyl protons. Furthermore, the ^{13}C NMR spectra revealed the presence of two additional signals; the first one at the range of 24.3–24.4 ppm due to the aliphatic methyl group at C-2 and a second signal at the range of 153.7–154.1 ppm assigned for the C-2. Whereas, the pyrrolo[3,2-*e*][1,4]diazepine derivatives **10a–c** were obtained by intramolecular cyclisation of compounds **7a–c** using potassium carbonate in dimethylformamide (Scheme 3). Finally, *N*-alkylation of compounds **10a–c** with ethyl chloroacetate afforded the ethyl ester derivatives **11a–c** using potassium carbonate in acetone (Scheme 3). The disappearance of the amidic protons (CONH) of the starting materials **10a–c** was observed in the ^1H NMR spectra of compounds **11a–c**, in addition to the

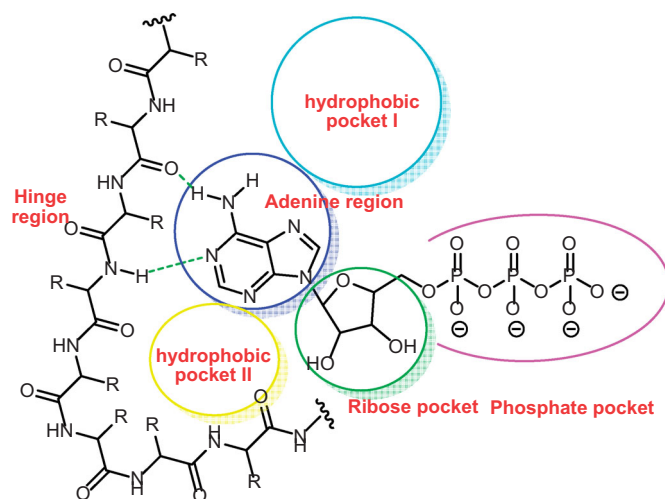


Figure 2. ATP binding site of EGFR cavity composed of five main parts^{47–49}.

presence of triplet signals at 1.28–1.29 ppm and quartette signals around 4.24 ppm due to the ethyl group. The ¹³C NMR spectra of compounds **11a–c** revealed three signals in the range of 159.6–167.6 ppm that were assigned for the carbon atoms of the three carbonyl groups.

2.2. Biological evaluation

2.2.1. Anticancer activity

Evaluation of the anticancer activity was performed against liver (Hep3B), colon (HCT116), and breast (MCF-7) cancer cell lines in the Centre of Genetic Engineering, Al-Azhar University, Cairo, Egypt, using Sulforhodamine-B (SRB) assay⁶⁵. Doxorubicin (DOX) was used as a reference drug. The survival curve was obtained by plotting concentrations of the compound under investigation against the survival fraction of the tumour cells. Then, results were expressed in half maximal inhibitory concentration (IC₅₀).

All the tested derivatives showed potent antiproliferative activities (IC₅₀ = 0.009–2.195 μM) against the three cancer cell lines (Table 1). A closer look at the results revealed that compound **8b** exhibited the highest cytotoxic activity against Hep3B and MCF-7 cell lines with IC₅₀ values of 0.049 and 0.043 μM, respectively. On the other hand, compound **8b** displayed the highest cytotoxic activity against the HCT116 cell line with IC₅₀ values of 0.011 μM.

2.2.2.1. Structure-Activity Relationship (SAR). Inspecting the results of the anti-proliferative activity of the designed candidates, we concluded a valuable SAR. With reference to their cytotoxic activity, it was noticed that counterparts incorporating 2,3-dihydro-1*H*-pyrrolizine moiety (scaffold A) were slightly more advantageous than the 3*H*-pyrimido[4,5-*b*]pyrrolizine derivatives (scaffold B). However, hexahydro-[1, 4]diazepino[5,6-*b*]pyrrolizine containing derivatives (scaffold C) displayed less potent inhibitory activity against the tested cell lines.

Concerning the di-aryl compounds **6a–c**, compound **6a** (unsubstituted-*N*-phenylcarbamoyl derivatives) displayed higher activity than **6b** and **6c** (4-methyl and 4-chloro-*N*-phenylcarbamoyl derivatives, respectively) against Hep3B (IC₅₀ = 0.219 μM) and HCT116 (IC₅₀ = 0.213 μM) cancer cell lines. While the methyl analogue **6b** was the most active member against MCF-7 cell line with IC₅₀ value of 0.336 μM. Replacement of the aromatic 6-(4-nitrobenzylidene)amino side chain in compounds **6a–c** by the 2-(piperidin-1-yl)acetamido moiety (compounds **8a–c**) resulted in a slightly

enhanced cytotoxicity; compounds **8a–c** showed IC₅₀ values in the range of 0.031–0.408 μM against the three cell lines. Among the three derivatives **8a–c**, the methyl derivative **8b** displayed the highest anticancer activity against the three cell lines.

Evaluation of the anticancer activity of pyrrolo[3,2-*d*]pyrimidine **9a–c**, revealed that the 4-chloro congener derivative **9c** was the most active against HCT116 cell line among all the tested compounds (IC₅₀ = 0.009 μM). While, the pyrrolo[3,2-*e*][1, 4]diazepine derivatives (compounds **11a–c**) showed comparable activity to their fused pyrrolo[3,2-*d*]pyrimidine analogues (**9a–c**) with enhancement in activity of the 4-chloro **11c** over **9c** against MCF-7 cell line (IC₅₀ = 0.364 versus 1.479 μM). Thus, the SAR study pointed out the significance of a single methyl group as it presents in the most active compounds **8b** (*N*-*p*-tolylcarbamoyl derivative) and **9a,c**; 2-methyl group on the fused pyrrolo[3,2-*d*]pyrimidine scaffold. However, the comparable activity among the three series (**A–C** scaffolds) is raising a query about the significance of the molecular modifications on the physicochemical properties, which could affect the cellular barriers positively.

2.2.2. EGFR and CDK-2 inhibitory activity

According to the anti-proliferative activity of the tested compounds, **8b** showed a substantial broad-spectrum activity against Hep3B, HCT116 and MCF-7 cell lines (IC₅₀ = 0.049, 0.031 and 0.043 μM, respectively). Thus, compound **8b** was tested for its inhibitory activity against both EGFR and CDK-2.

The results revealed that compound **8b** showed excellent activity against CDK2 with an inhibition value of 15% compared to the reference molecule, imatinib (2%). On the other hand, it showed less activity against EGFR (% Inhibition = –70%) compared to imatinib (% Inhibition = –13%) (Table 2).

2.2.3. Kinase profiling test

The previous results encouraged us to test compound **8b** against other different kinases (18 kinases) to reach a good insight into its kinases inhibitory profile. The result showed that compound **8b** has good inhibitory activity against DYRK3 and GSK3 alpha kinases. For its activity against DYRK3, it showed an inhibition value of 23% compared to imatinib (% Inhibition = 10%). Regarding its activity against GSK3 alpha, it showed an inhibition value of 10% compared to imatinib (% Inhibition = 1%).

Additionally, compound **8b** showed imatinib comparable activity against ALK1, AMPK (A1/B1/G1), GRK1, MSK1, p38 Alpha, PDK1, and PRKG1. On the other hand, it showed moderate to weak activity against CK1 Alpha 1, Aurora A, BLK, BRAF, ASK1, EPHA1, FLT1, NEK1, and SGK1 (Table 2).

2.2.4. Determination of cell cycle perturbations

To study the mechanistic actions regarding compounds **6a** and **8b**, cell cycle analyses using flow cytometry (BC, FC500) were performed. The results of the cell cycle perturbation of the MCF-7 cell line treated with compounds **6a** and **8b** (72 h, separately) were presented in Figures 4 and 5, respectively. Each of the two compounds caused a three-fold increase of cells in the S phase at 1 μM compared to control. This increase in the S-phase cell population was accompanied by a concomitant decrease in the G₁ cell population. However, there was no considerable change in the S phase cellular population at 5 and 10 μM, which means that the effect of compounds **6a** and **8b** are not dose-dependent.

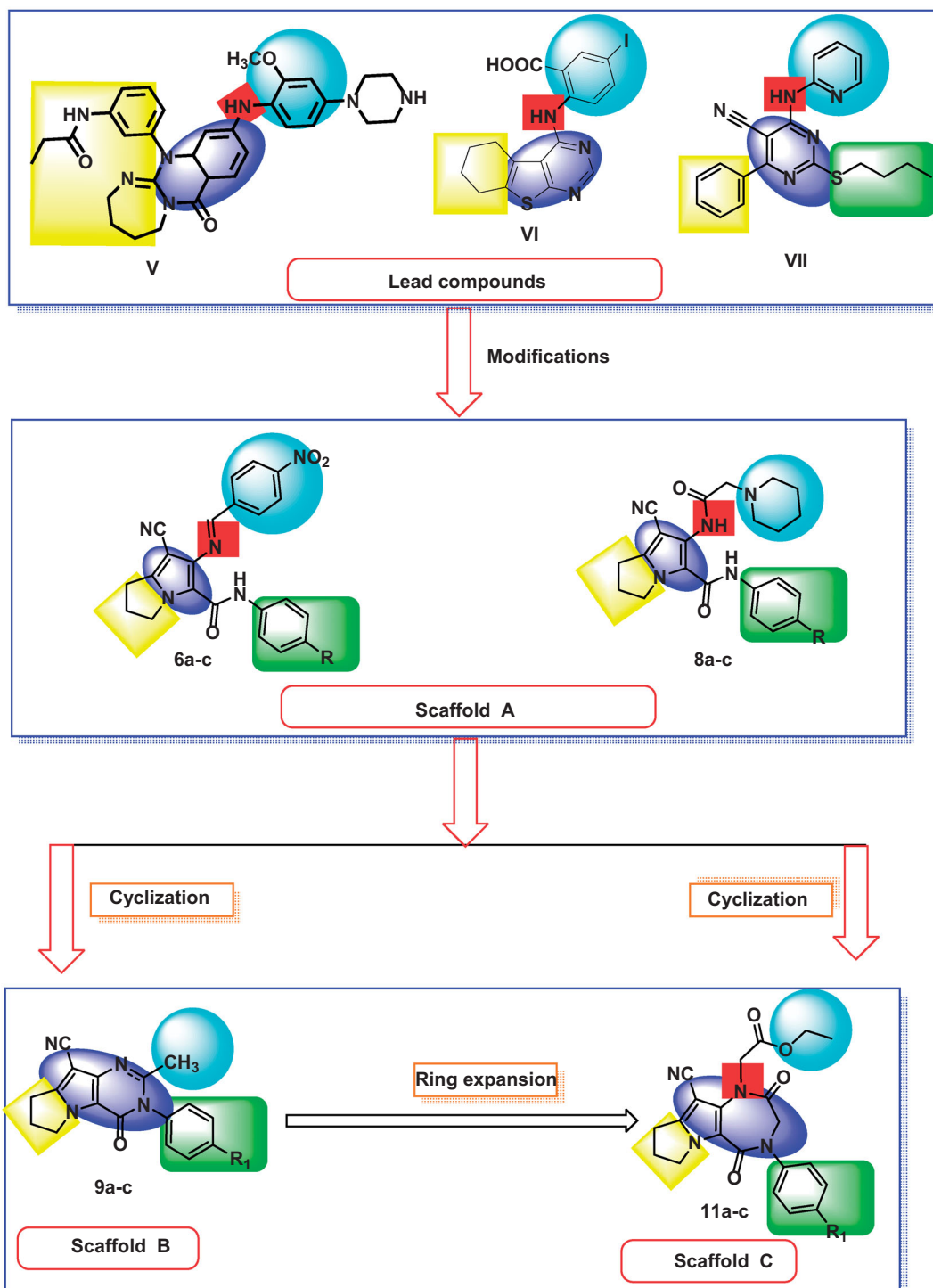


Figure 3. Design strategies of Scaffolds A, B and C.

2.3. In silico studies

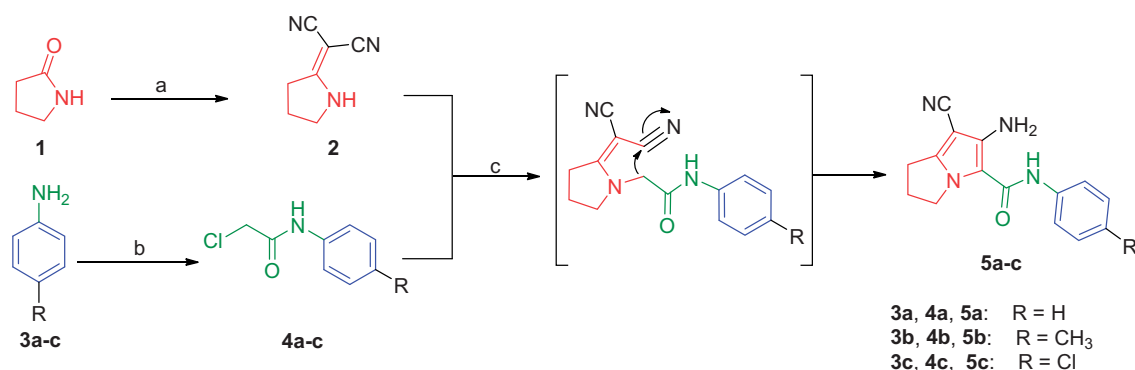
2.3.1. Docking studies

A docking study was conducted in the hopes of learning more about how the synthesised compounds interact with their targets^{67–69}. EGFR (PDB: 4HJO), CDK-2 (PDB: 6GUH), DYRK3 (PDB: 5Y86), and GSK3 (PDB: 5HLP) were employed as biological targets in docking investigations utilising MOE 14.0 software. The co-crystallised ligands (erlotinib and AZD5438) were utilised as anti-EGFR and anti-CDK-2 reference compounds respectively. When compared to the reference molecules, the docking results

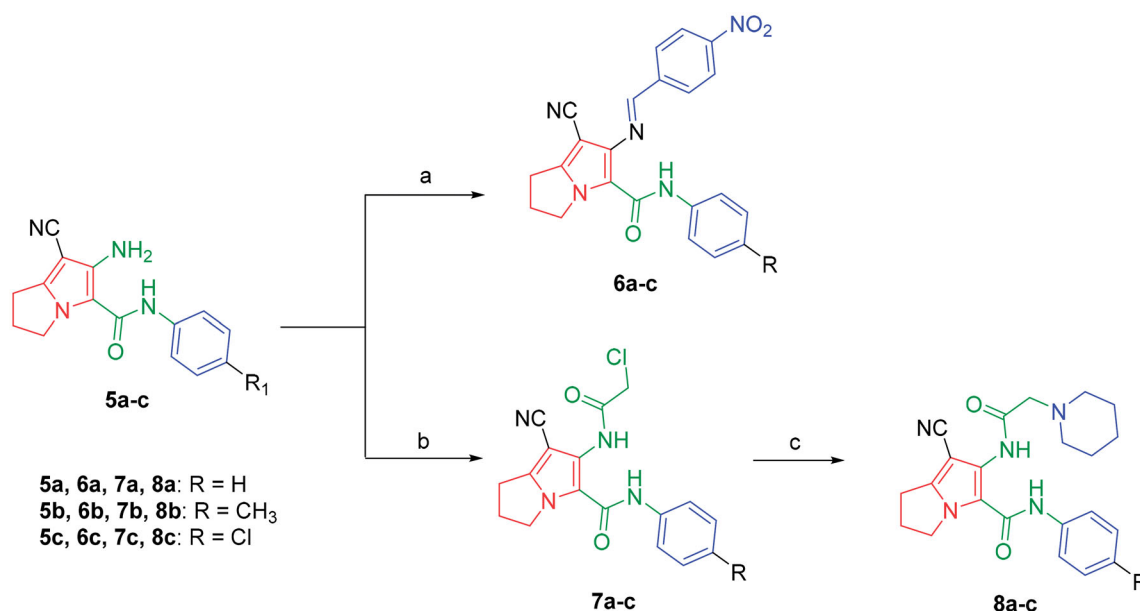
demonstrated that the synthesised compounds have a high affinity for the two examined targets (Table 3).

Redocking of co-crystallised ligands (Erlotinib and AZD5438) against EGFR and CDK-2, respectively, was used to validate docking experiments. Erlotinib and AZD5438 had RMSDs of 0.88 and 0.54 Å for docked and original ligands, respectively. The validity of the docking operation is shown by these values (Figure 6).

The binding energy of erlotinib was found to be -23.49 kcal/mol. The quinazoline molecule was buried in the adenine pocket, creating a hydrogen connection with Met769. Furthermore,



Scheme 1. Construction of compounds **5a–c**. Reagents and conditions: (a) (CH₃)₂SO₄, benzene, CH₂(CN)₂, reflux, 6 h; (b) ClCH₂COCl, glacial acetic acid, CH₂COONa, 30–40 °C, 2 h; (c) acetone, K₂CO₃, reflux, 24 h.



Scheme 2. Synthesis of compounds **6a–c**, **7a–c** and **8a–c**. Reagents and conditions: (a) 4-Nitrobenzaldehyde, absolute ethanol, glacial acetic acid; (b) ClCH₂COCl, benzene; r.t.; 48 h; (c) piperidine, NaHCO₃, absolute ethanol, reflux, 8 h.

Lue694, Ala719, and Leu820 established four hydrophobic contacts with quinazoline. The ethynylphenyl moiety was positioned in the hydrophobic pocket I, resulting in three hydrophobic interactions with Ala719, Val702, and Lys721. The 2-methoxyethoxy groups formed a hydrogen bond with Cys773 in the hydrophobic region II (Figure 7).

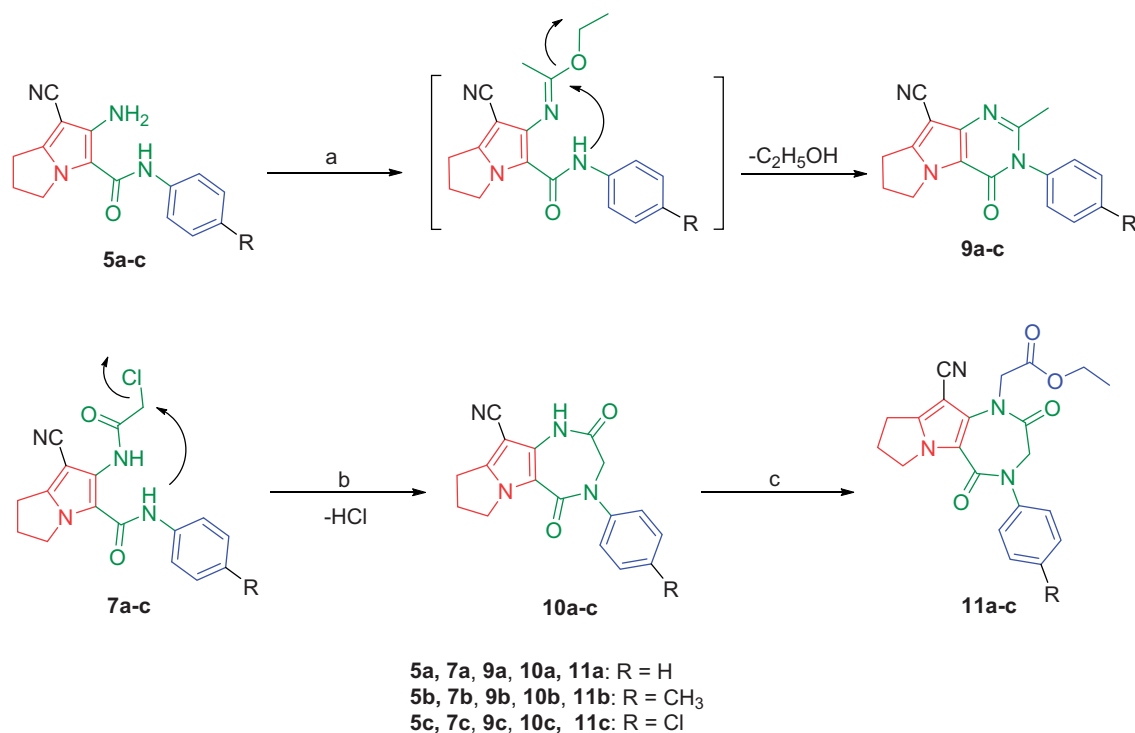
Compound **8b** showed a binding mode like that of erlotinib with a binding energy of -22.46 kcal/mol. The 1*H*-pyrrole-3-carbonitrile moiety occupied the adenine pocket of the EGFR forming three hydrophobic interactions with Leu820, Leu694, and Val702. Piperidine moiety was oriented into the hydrophobic pocket I to form one hydrophobic interaction with Leu694. The pyrrolidine moiety occupied the hydrophobic pocket II forming one hydrophobic interaction with Lys721 in close contact with Thr766, Leu764, and Leu834. Moreover, *p*-tolyl moiety occupied the ribose binding pocket forming one electrostatic attraction with Cys773 (Figure 8).

The co-crystallised ligand (AZD5438) showed binding energy of -21.66 kcal/mol against CDK-2. The pyrimidine moiety occupied the adenine pocket forming three hydrophobic bonds with Leu134, and Ala31, Val64. The NH-linker formed one hydrogen bond with Leu83. The terminal methylsulfonyl benzene moiety occupied the hydrophobic pocket forming a hydrogen bond with

Asp86 and one hydrophobic interaction with Ile10. Additionally, the 1-isopropyl-2-methyl-1*H*-imidazole moiety occupied the other hydrophobic region forming a hydrogen bond with Lys33. Also, it formed four hydrophobic interactions with Leu134 and Val18 (Figure 9).

Compound **8b** showed a binding mode like that of AZD543 with a binding energy of -24.52 kcal/mol. The 1*H*-pyrrole-3-carbonitrile moiety occupied the adenine pocket forming two hydrophobic interactions with Leu134 and Val18. The pyrrolidine moiety was oriented into the hydrophobic pocket forming three hydrophobic interactions with Val18, Lys33, and Ala31. The piperidine moiety occupied another hydrophobic pocket forming one hydrophobic interaction with Lys89 in close contact with Asp86 and Gln85. The two amide linkers formed one hydrogen bond and one electrostatic interaction with Ile10. Moreover, *p*-tolyl moiety occupied the ribose binding pocket forming one hydrophobic interaction with Gly13 (Figure 10).

Docking calculations between compound **8b** and DYRK3 and GSK3 revealed that it could occupy the active sites and interact with the key amino acids of each enzyme (Figure 11 and Figure 12) with the binding energy of -24.54 and -16.85 kcal/mol, respectively. The binding free energy of the co-crystallised ligands of DYRK3 (HRM) and GSK3 (65 A) was calculated to be -20.80 and



Scheme 3. Synthesis of compounds **9a-c**, **10a-c** and **11a-c**. Reagents and conditions: (a) Excess $\text{CH}_3\text{C}(\text{OC}_2\text{H}_5)_3$, reflux, 12 h; (b) K_2CO_3 , DMF, r.t., 48 h; (c) $\text{ClCH}_2\text{COOC}_2\text{H}_5$, K_2CO_3 , acetone, reflux, 6 h.

–16.41 kcal/mol, respectively and the binding modes were presented in [Supplementary data](#).

2.3.2. In silico toxicity prediction

In this work, eight toxicity parameters were estimated computationally depending on the constructed toxicity models in Discovery studio software^{70–72}. The results revealed that the calculated toxicity potential of the synthesised compound was low. Except for compound **6a**, all compounds were non-carcinogenic for mouse females based on the FDA rodent carcinogenicity model. In addition, compounds **6a**, **8a**, **8b**, **9a**, and **11a** showed carcinogenic potency TD_{50} values ranging from 11.774 to 71.541 mg/kg body weight/day, which were higher than that of erlotinib (8.057 mg/kg body weight/day). All compounds had rat maximum tolerated dose values less than that of erlotinib (0.083 g/kg body weight) except compound **8c** (0.107 g/kg body weight). For the rat oral LD_{50} model, except compounds **9a** and **9c**, all compounds showed oral LD_{50} values higher than that of erlotinib (0.662 mg/kg body weight/day). In addition, all compounds exhibited rat chronic LOAEL values higher than that of erlotinib (0.036 mg/kg body weight/day) except compounds **8c** and **11c**. Moreover, all the tested compounds were predicted to be mild irritants in the ocular irritancy model, and non-irritants in the skin irritancy model ([Table 4](#)).

2.3.3. ADMET studies

ADMET parameters were predicted using discovery studio software^{69,73–75}. Erlotinib was used as a reference compound. The predicted ADMET parameters were listed in [Table 5](#). The results revealed that compounds **6a-c** had very low Blood Brain Barrier penetration power. Compounds **8a-c** and **11a-c** were anticipated to have low levels of BBB penetration. On the other hand, compound **9a-c** was predicted to have medium levels of BBB penetration. Accordingly, the synthesised compounds were expected to

be safe for CNS. The predicted aqueous solubility of the synthesised compounds ranged from good to low. All the synthesised compounds showed good absorption levels except compounds **6a** and **6b** which showed moderate absorption levels. All the synthesised members were predicted as non-inhibitors of CYP2D6. Additionally, all of them were expected to bind plasma protein by more than 90% ([Figure 13](#)).

3. Conclusion

In this work new compounds having the essential pharmacophoric features of EGFR inhibitors were designed and synthesised. Three series of 1*H*-pyrrole, pyrrolo[3,2-*d*]pyrimidine and pyrrolo[3,2-*e*][1,4]diazepine derivatives were obtained. Compound **9c**, the fused pyrrolo[4,5-*b*]pyrrolizine derivative, showed selectivity towards the HCT116 colon cancer cell line with activity comparable with that of DOX ($\text{IC}_{50} = 0.009$ and $0.008 \mu\text{M}$, respectively). While compound **8b**, the 1*H*-pyrrole derivative featuring the extended 2-(piperidin-1-yl)acetamido moiety at C-6, showed a broad-spectrum inhibition against Hep3B, HCT116 and MCF-7 cell lines ($\text{IC}_{50} = 0.049$, 0.031 and $0.043 \mu\text{M}$, respectively). Regarding compound **8b**, the kinase profiling evaluations revealed its inhibitory activity against three types of kinases: CDK2/Cyclin A1, DYRK3 and GSK3 alpha. Therefore, this study reinforces the promising anticancer efficacy of 1*H*-pyrrole pyrrolo[3,2-*d*]pyrimidine derivatives based on their multi-targets activity, which were supported by molecular modelling characteristics. Add to that, their superior predicted safety and predicted pharmacokinetic properties as drug-like or lead-like molecules.

4. Experimental protocol

4.1. Chemistry

All details of chemical reagents and apparatus were described in [Supplementary Data](#). Compounds **2**⁶¹, **4a-c**⁶³, **5a-c**⁶³, **7a-c**

Table 1. IC₅₀ values of the new compounds (**6a–c**, **8a–c**, **9a–c**, and **11a–c**) against Hep3B, HCT116 and MCF-7 cell lines.

Comp.	Scaffold	R	Spacer	R ₁	IC ₅₀ (μM)		
					Hep3B	HCT116	MCF-7
6a	A	H	N = CH-		0.219	0.213	0.422
6b	A	CH ₃	N = CH-		1.956	2.069	0.336
6c	A	Cl	N = CH-		1.470	0.955	2.195
8a	A	H	-NHCOCH ₂ -		0.313	0.408	0.315
8b	A	CH ₃	-NHCOCH ₂ -		0.049	0.031	0.043
8c	A	Cl	-NHCOCH ₂ -		0.144	0.180	0.294
9a	B	H	-	-	0.487	0.011	0.137
9b	B	CH ₃	-	-	0.265	0.820	0.644
9c	B	Cl	-	-	0.072	0.009	1.479
11a	C	H	-	-	0.218	0.840	0.154
11b	C	CH ₃	-	-	0.271	0.303	0.354
11c	C	Cl	-	-	0.179	0.286	0.364
DOX	-	-	-	-	0.005	0.008	0.008

Hep3B, Liver cancer cell line; HCT116, colon cancer cell line; MCF-7, breast cancer cell line; DOX, doxorubicin.

Table 2. Inhibitory activity of compound **8b** and imatinib against 20 kinases at 10 μM⁶⁶.

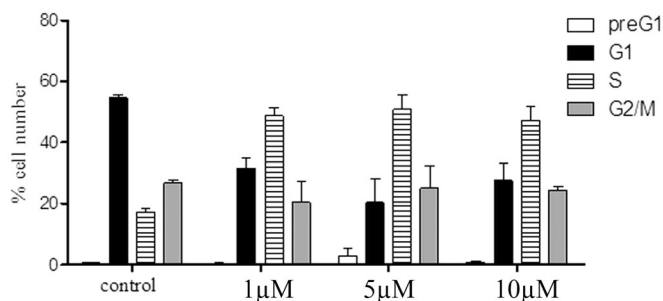
Kinase	% Inhibition		Kinase	% Inhibition	
	Imatinib ^a	8b ^b		Imatinib ^a	8b ^b
AMPK (A1/B1/G1)	-14%	-18%	EPHA1	-22%	-46%
ALK1	-18%	-21%	FLT1	10%	-8%
ASK1	-5%	-23%	GRK1	-2%	-1%
Aurora A	-38%	-6%	GSK3 alpha	1%	10%
BLK	-3%	-36%	MSK1	-49%	-48%
BRAF	-13%	-77%	NEK1	2%	-8%
CDK2/Cyclin A1	2%	15%	p38 Alpha	-17%	-23%
CK1 Alpha 1	0%	-10%	PDK1	-34%	-28%
DYRK3	10%	23%	PRKG1	-4%	-4%
EGFR	-13%	-70%	SGK1	-3%	-10%

The +ve values indicate the inhibition % and -ve values indicate increase in enzyme activity.

and **10a–c**⁷⁶ were prepared using the previously reported methods.

4.1.1. General method for preparation of compounds (**6a–c**)

To a solution of 4-nitrobenzaldehyde (3.75 mmol) in absolute ethanol (20 ml), the pyrrolizines **5a–c** (3.75 mmol) and 0.5 ml of glacial

**Figure 4.** Cell cycle distribution of MCF-7 treated with compound **6a** (μM, 72 h; x axis); % cell (y axis).

acetic acid were added. The reaction mixture was refluxed for 4 h. The reaction mixture was left to cool. The products **6a–c** were crystallised out as orange crystals and recrystallized from ethanol

4.1.2. (E)-7-Cyano-6-((4-nitrobenzylidene)amino)-N-phenyl)-2,3-dihydro-1H-pyrrolizine-5-carboxamide (6a). The title compound was obtained from compound **5a** as orange crystals, m.p. 278–80 °C, yield 76%, IR_{max}/cm⁻¹ 3279 (NH), 3076 (C-H aromatic), 2935, 2852 (CH₂), 2210 (CN), 1658 (CO), 1601 (C=N), 1548, 1469

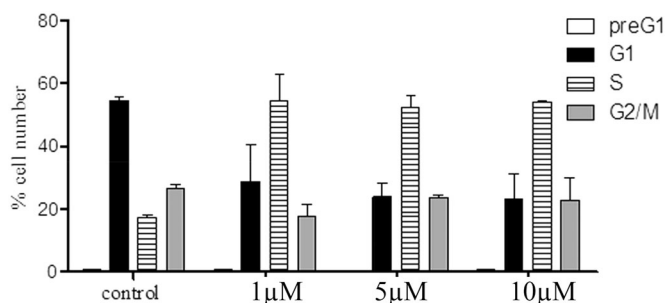


Figure 5. Cell cycle distribution of MCF-7 treated with compound **8b** (μM , 72 h: x axis); % cell (y axis).

Table 3. The binding free energies of the synthesised compounds against EGFR and CDK-2.

Comp.	Binding free energy (kcal/mol)	
	EGFR	CDK-2
6a	-18.33	-23.67
6b	-18.97	-23.84
6c	-19.14	-23.60
8a	-20.67	-24.89
8b	-22.46	-24.52
8c	-20.08	-24.20
9a	-17.69	-17.77
9b	-18.90	-17.74
9c	-17.72	-16.71
11a	-21.54	-24.08
11b	-23.30	-24.18
11c	-18.93	-23.98
Erlotinib	-23.49	-
AZD5438	-	-21.66

(C=C, NH), 1412, 1337 (C-N, C-O). ^1H NMR (CDCl_3 , 400 MHz): δ 2.60 (m, 2H, CH_2 -2), 3.07 (t, 2H, $J=7.4$ Hz, CH_2 -1), 4.57 (t, 2H, $J=7.4$ Hz, CH_2 -3), 7.17 (t, 1H, $J=8.2$ Hz, CH-4'), 7.41 (t, 2H, $J=8.2$ Hz, CH-3', -5'), 7.62 (d, 2H, $J=8.2$ Hz, CH-2', -6'), 8.1 and 8.41 (two d, 4H, $J=8$ Hz, CH-2'', -3'', -4'', -5'', -6''), 9.28 (s, H, N=CH) and 10.40 (s, 1H, NH, disappeared on deuteration). ^{13}C NMR (CDCl_3 , 100 MHz): δ 24.5, 25.4, 50.4, 76.7, 116.0, 119.1, 119.6, 124.4, 124.4, 129.1, 129.3, 137.8, 137.9, 140.9, 148.9, 149.7, 156.4, 158. MS (EI): m/z (%) 400 ($\text{M}^+ + 1$, 13), 399 (M^+ , 35), 307 (100). Anal. Calcd. for $\text{C}_{22}\text{H}_{17}\text{N}_5\text{O}_3$ (399.40): C, 66.16; H, 4.29; N, 17.53. Found: C, 68.35; H, 4.15; N, 17.23.

4.1.3. (E)-7-Cyano-6-((4-nitrobenzylidene)amino)-N-(4-tolyl)-2,3-dihydro-1H-pyrrrolizine-5-carboxamide (6b). The title compound was obtained from compound **5b** as orange crystals, m.p. 291–3 °C, yield 79%, $\text{IR}_{\text{max}}/\text{cm}^{-1}$ 3280 (NH), 3069 (C-H aromatic), 2918 (CH_3 , CH_2), 2210 (CN), 1657 (CO), 1601 (C=N), 1544, 1519 (C=C, N-H), 1411, 1338 (C-N, C-O). ^1H NMR (CDCl_3 , 400 MHz): δ 2.37 (s, 3H, CH_3 Ph), 2.60 (m, 2H, CH_2 -2), 3.10 (t, 2H, $J=7.4$ Hz, CH_2 -1), 4.59 (t, 2H, $J=7.4$ Hz, CH_2 -3), 7.21 (d, 2H, $J=8.4$ Hz, CH-3', -5'), 7.53 (d, 2H, $J=8.4$ Hz, CH-2', -6'), 8.10 (d, 2H, $J=8.4$ Hz, CH-2'', -6''), 8.39 (d, 2H, $J=8.4$ Hz, CH-3'', -5''), 9.28 (s, H, N=CH) and 10.37 (s, 1H, NH, disappeared on deuteration). ^{13}C NMR (CDCl_3 , 100 MHz): δ 20.9, 24.5, 25.5, 50.3, 76.7, 116.1, 119.3, 119.6, 124.4, 129.1, 129.8, 134.1, 135.4, 137.7, 140.9, 148.7, 149.6, 156.3, 157.9. MS (EI): m/z (%) 414 ($\text{M}^+ + 1$, 15), 413 (M^+ , 51), 307 (100). Anal. Calcd. for $\text{C}_{23}\text{H}_{19}\text{N}_5\text{O}_3$ (413.43): C, 66.82; H, 4.63; N, 16.94. Found: C, 67.01; H, 4.58; N, 16.91.

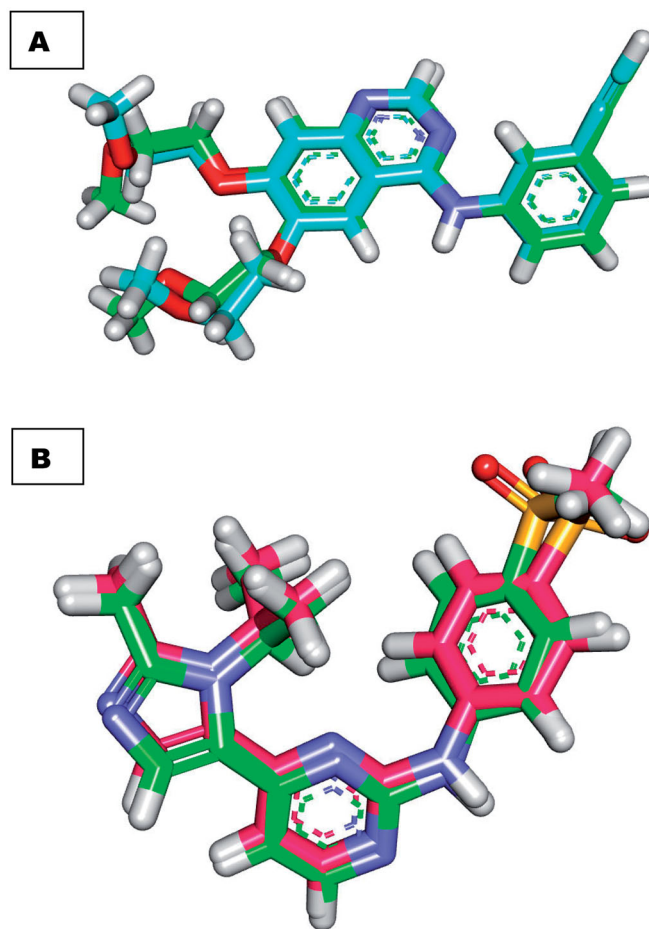


Figure 6. (A) superimposition of the docked ligand of erlotinib (turquoise) and the original ligand (green) with an RMSD value of 0.88 Å. (B) superimposition of the docked ligand of AZD5438 (pink) and the original ligand (green) with RMSD value of 0.54 Å.

4.1.4. (E)-N-(4-Chlorophenyl)-7-cyano-6-((4-nitrobenzylidene)amino)-2,3-dihydro-1H-pyrrrolizine-5-carboxamide (6c). The title compound was obtained from compound **5c** as yellow crystals, m.p. 283–5 °C, yield 83%, $\text{IR}_{\text{max}}/\text{cm}^{-1}$ 3245 (NH), 3111 (C-H aromatic), 2968 (CH_2), 2214 (CN), 1680 (CO), 1597 (C=N), 1541, 1482 (C=C, NH), 1412, 1344 (C-N, C-O), 836, 754 (C-Cl). ^1H NMR (CDCl_3 , 400 MHz): δ 2.63 (m, 2H, CH_2 -2), 3.11 (t, 2H, $J=7.4$ Hz, CH_2 -1), 4.58 (t, 2H, $J=7.4$ Hz, CH_2 -3), 7.38 (d, 2H, $J=8.4$ Hz, CH-3', -5'), 7.60 (d, 2H, $J=8.4$ Hz, CH-2', -6'), 8.10 (d, 2H, $J=8.4$ Hz, CH-2'', -6''), 8.42 (d, 2H, $J=8.4$ Hz, CH-3'', -5''), 9.31 (s, H, N=CH) and 10.45 (s, 1H, NH, disappeared on deuteration). ^{13}C NMR (CDCl_3 , 100 MHz): δ 24.5, 25.4, 50.4, 76.7, 115.9, 119.2, 119.8, 124.4, 129.1, 129.3, 135.4, 137.6, 137.7, 140.9, 148.9, 149.7, 156.4, 157.9. MS (EI): m/z (%) 435 ($\text{M}^+ + 2$, 74), 433 (M^+ , 76), 405 (100). Anal. Calcd. for $\text{C}_{22}\text{H}_{16}\text{ClN}_5\text{O}_3$ (433.85): C, 60.91; H, 3.72; N, 16.14. Found: C, 61.10; H, 3.68; N, 16.11.

4.1.5. General method for preparation of compounds (8a–c)

A mixture of compounds **7a–c** (2.91 mmol), piperidine (0.5 g, 5.9 mmol) and dry sodium bicarbonate (0.5 g, 5.9 mmol) in absolute ethanol (10 ml) was refluxed for 8 h. Then, the reaction mixture was filtered while hot, and the produced white crystals upon concentration were collected, dried, and recrystallized from ethanol.

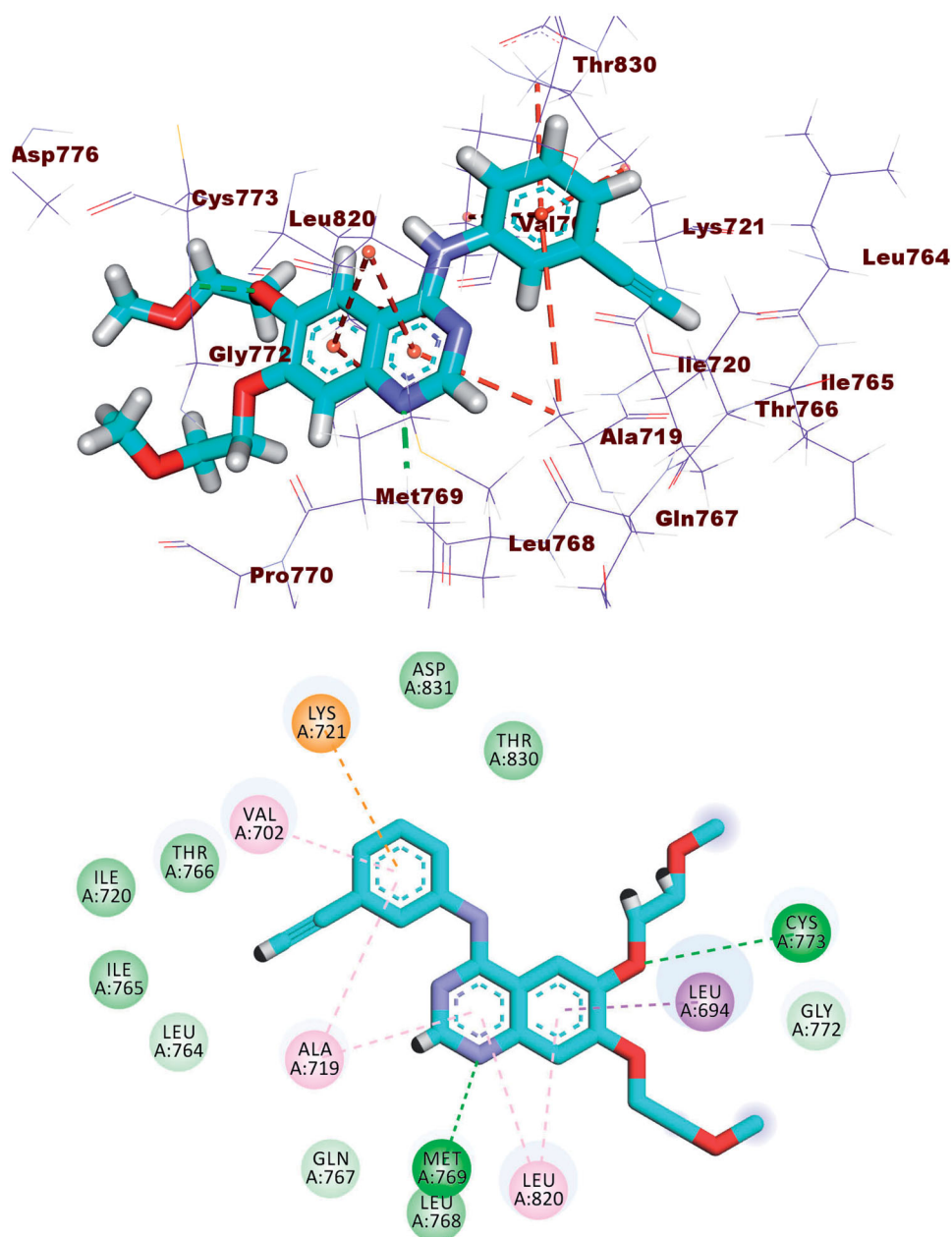


Figure 7. Erlotinib docked into the active site of EGFR.

4.1.5.1. 7-Cyano-N-phenyl-6-(2-(piperidin-1-yl)acetamido)-2,3-dihydro-1H-pyrrolizine-5-carboxamide (8a). The title compound was obtained from compound **7a** as white crystals, m.p. 205–7 °C, yield 72%, $\text{IR}_{\text{max}}/\text{cm}^{-1}$ 3243, 3130 (NHs), 3060 (C-H aromatic), 2935, 2852 (CH_2), 2220 (CN), 1660 (COs), 1601, 1557, 1493 (C=C, NH), 1451, 1390, 1319 (C-N, C-O). ^1H NMR (CDCl_3 , 400 MHz): δ 1.5 (m, 2H, CH_2 -4''), 1.7 (m, 4H, CH_2 -3'', -5''), 2.54 (m, 2H, CH_2 -2), 2.69 (t, 4H, $J=5.2$ Hz, CH_2 -2'', -6''), 3.02 (t, 2H, $J=7.6$ Hz, CH_2 -1), 3.27 (s, 2H, COCH_2), 4.40 (t, 2H, $J=7.2$ Hz, CH_2 -3), 7.12 (t, 1H, $J=8$ Hz, CH -4'), 7.34 (t, 2H, $J=8$ Hz, CH -3', -5'), 7.6 (d, 2H, $J=8$ Hz, CH -2', CH -6'), 9.44 (s, H, NHCOCH_2 , which disappeared on deuteration) and 9.80 (s, H, CONH phenyl, which disappeared on deuteration). ^{13}C NMR (CDCl_3 , 100 MHz): δ 23.5, 25, 25.7, 26.1, 49.6, 55.1, 62.1, 83.9, 114, 119.5, 120.3, 124.1, 124.4, 129, 138.3, 145.7, 157.6, 173.2. MS (EI): m/z (%) 392 (M^++1 , 57), 391 (M^+ , 67), 138 (100). Anal. Calcd. for $\text{C}_{22}\text{H}_{25}\text{N}_5\text{O}_2$ (391.47): C, 67.50; H, 6.44; N, 17.89. Found: C, 67.80; H, 6.72; N, 17.67.

4.1.5.2. 7-Cyano-6-(2-(piperidin-1-yl)acetamido)-N-(4-tolyl)-2,3-dihydro-1H-pyrrolizine-5-carboxamide (8b). The title compound was obtained from compound **7b** as white crystals, m.p. 178–80 °C, yield 72%, $\text{IR}_{\text{max}}/\text{cm}^{-1}$ 3240, 3186 (NHs), 3064 (C-H aromatic), 2983, 2930, 2853 (CH_3 , CH_2), 2222 (CN), 1656 (COs), 1604, 1547, 1513 (C=C, NH), 1455, 1385, 1321 (C-N, C-O). ^1H NMR (CDCl_3 , 400 MHz): δ 1.51 (m, 2H, CH_2 -4''), 1.72 (m, 4H, CH_2 -3'' -5''), 2.33 (s, 3H, CH_3 Ph), 2.54 (m, 2H, CH_2 -2), 2.70 (t, 4H, $J=5.2$ Hz, CH_2 -2'' -6''), 3.02 (t, 2H, $J=7.4$ Hz, CH_2 -1), 3.28 (s, 2H, COCH_2), 4.39 (t, 2H, $J=7.2$ Hz, CH_2 -3), 7.13 (d, 2H, $J=8$ Hz, CH -3', -5'), 7.49 (d, 2H, $J=8$ Hz, CH -2', -6'), 9.42 (s, H, NHCOCH_2 , disappeared on deuteration) and 9.69 (s, H, CONH phenyl, disappeared on deuteration). ^{13}C NMR (CDCl_3 , 100 MHz): δ 20.9, 23.5, 25.1, 25.7, 26.1, 49.5, 55.1, 62, 83.9, 114.1, 119.5, 120.4, 124.2, 129.5, 133.8, 135.8, 145.6, 157.5, 173.2. MS (EI): m/z (%) 407 (M^++2 , 69), 406 (M^++1 , 82), 405 (M^+ , 68) 148 (100). Anal. Calcd. for $\text{C}_{23}\text{H}_{27}\text{N}_5\text{O}_2$ (405.49): C, 68.13; H, 6.71; N, 17.27. Found: C, 68.33; H, 6.59; N, 17.50.

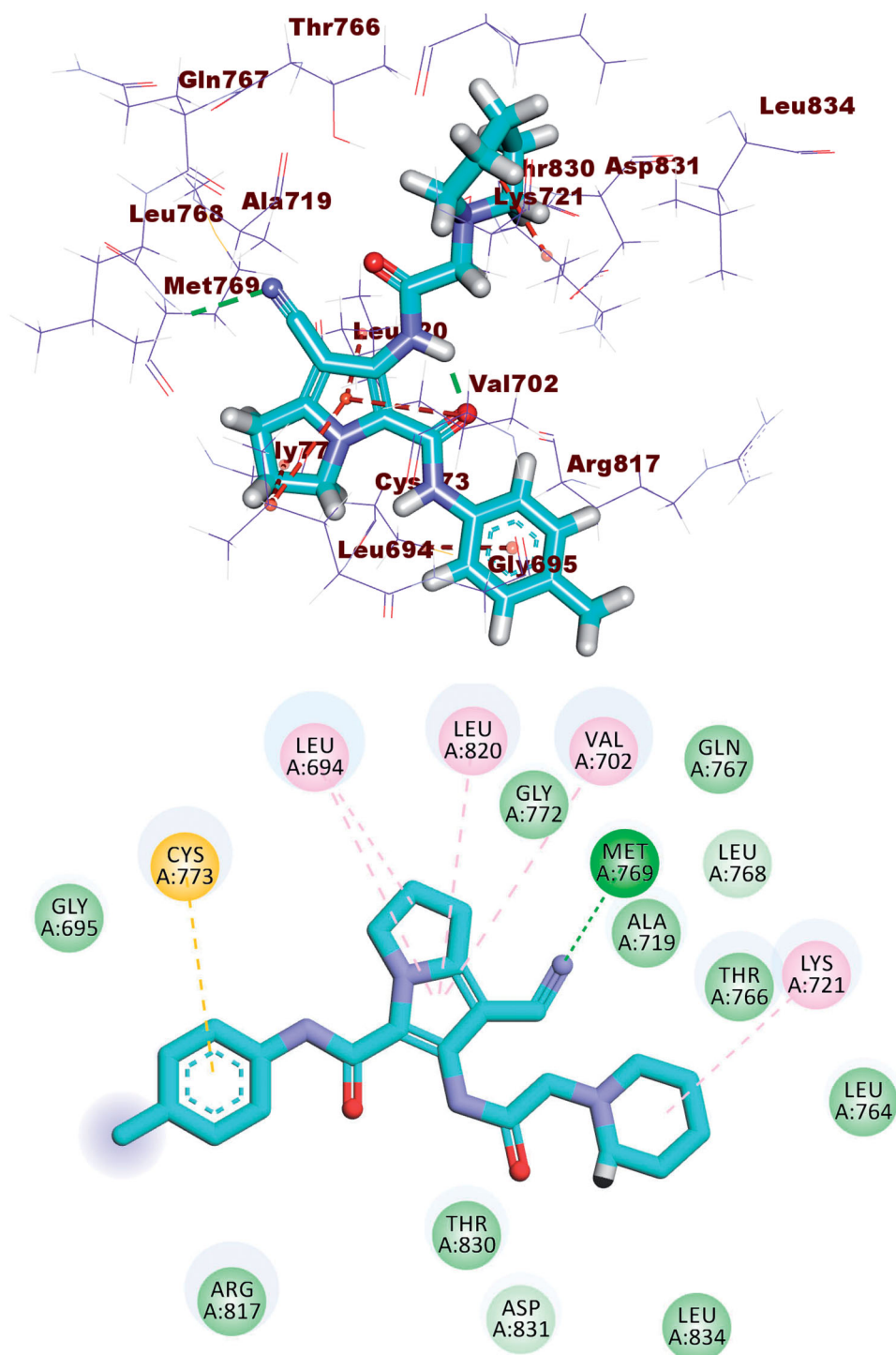


Figure 8. Compound **8b** docked into the active site of EGFR.

4.1.5.3. *N*-(4-Chlorophenyl)-7-cyano-6-(2-(piperidin-1-yl)acetamido)-2,3-dihydro-1H-pyrrolizine-5-carboxamide (**8c**). The title compound was obtained from compound **7c** as white crystals, m.p. 210–2 °C, yield 74%, $\text{IR}_{\text{max}}/\text{cm}^{-1}$ 3233, 3179 (NHs), 3053 (C-H aromatic), 2986, 2932 (CH_2), 2222 (CN), 1658 (COs), 1602, 1546 (C=C, NH), 1489, 1456, 1387 (C-N, C-O), 829, 792 (C-Cl). ^1H NMR (CDCl_3 , 400 MHz): δ 1.51 (m, 2H, CH_2 -4''), 1.74 (m, 4H, CH_2 -3''–5''), 2.55 (m, 2H, CH_2 -2), 2.74 (t, 4H, $J=5.2$ Hz, CH_2 -2''–6''), 3.02 (t, 2H, $J=7.4$ Hz, CH_2 -1), 3.32 (s, 2H, COCH_2), 4.39 (t, 2H, $J=7.4$ Hz, CH_2 -3), 7.28–7.58 (4H, aromatic protons), 9.41 (s, H, NHCOCH_2 , disappeared on deuteration) and 9.93 (s, H, CONH phenyl, disappeared

on deuteration). ^{13}C NMR (CDCl_3 , 100 MHz): δ 23.4, 25, 25.6, 26.1, 49.5, 55, 62, 83.9, 113.9, 120, 120.7, 124.4, 129, 131.6, 136.9, 145.8, 157.6, 173.3. MS (EI): m/z (%) 426 (M^++1 , 0.9), 98 (100). Calcd. for $\text{C}_{22}\text{H}_{24}\text{ClN}_5\text{O}_2$ (425.91): C, 62.04; H, 5.68; N, 16.44. Found: C, 62.30; H, 5.90; N, 16.15.

4.1.6. General method for preparation of compounds (9a–c)

A mixture of 6-amino-7-cyano-*N*-phenyl-2,3-dihydro-1H-pyrrolizine-5-carboxamide **5a–c** (3.75 mmol) and excess triethyl orthoformate was refluxed for 12 h. The solvent was then removed using a

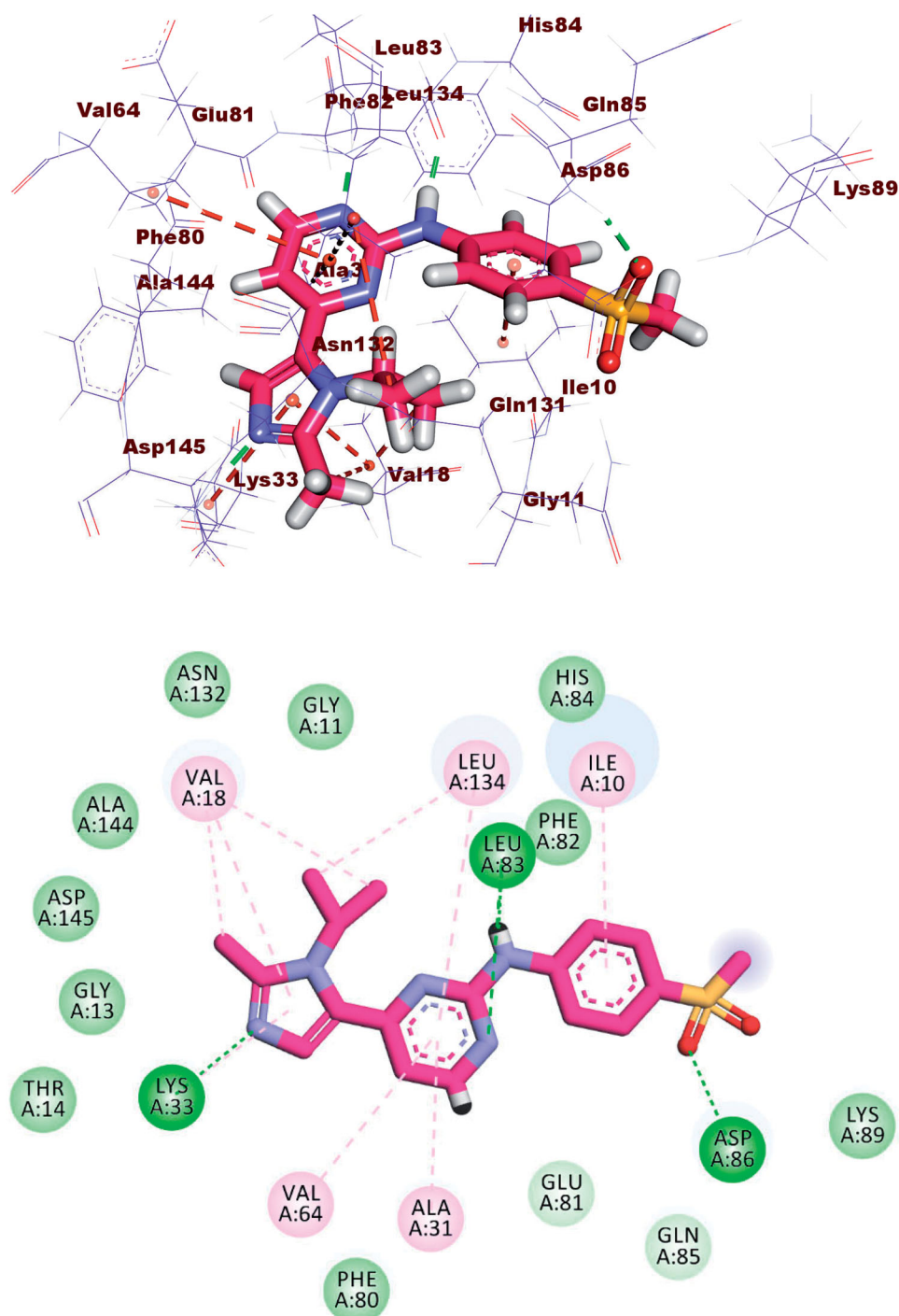


Figure 9. Co-crystallised ligand (AZD5438) docked into the active site of CDK-2.

rotary evaporator and the obtained residue was crystallised from ethanol.

4.1.6.1. Methyl-4-oxo-3-phenyl-4,6,7,8-tetrahydro-3H-pyrimido[4,5-b]pyrrolizine-9-carbonitrile (9a). The title compound was obtained from compound **5a** as white crystals, m.p. 243–5 °C, yield 55%, $\text{IR}_{\text{max}}/\text{cm}^{-1}$ 3061 (C-H aromatic), 2966, 2918 (CH_3 , CH_2), 2214 (CN), 1693 (CO), 1524 (C=C), 1421, 1304 (C-N, C-O). ^1H NMR (CDCl_3 , 400 MHz): δ 2.26 (s, 3H, $\text{CH}_3\text{C}=\text{N}$), 2.67 (m, 2H, CH_2 -7), 3.19 (t, 2H, $J=7.4$ Hz, CH_2 -8), 4.40 (t, 2H, $J=7.2$ Hz, CH_2 -6), 7.25 (d, 2H, $J=8$ Hz, CH-2', -6') and 7.51–7.59 (m, 3H, CH-3', -4', -5'). ^{13}C

NMR (CDCl_3 , 100 MHz): δ 24.3, 25.1, 26.2, 48, 81.1, 113.4, 113.9, 128, 129.4, 130, 137.3, 148.4, 152.3, 154.1, 154.3. MS (EI): m/z (%) 291 (M^++1 , 3), 290 (M^+ , 15), 85 (100). Anal. Calcd. for $\text{C}_{17}\text{H}_{14}\text{N}_4\text{O}$ (290.32): C, 70.33; H, 4.86; N, 19.30. Found: C, 70.12; H, 4.90; N, 19.41.

4.1.6.2. 2-Methyl-4-oxo-3-(4-tolyl)-4,6,7,8-tetrahydro-3H-pyrimido[4,5-b]pyrrolizine-9-carbonitrile (9b). The title compound was obtained from compound **5b** as white crystals, m.p. 251–3 °C, yield 59%, $\text{IR}_{\text{max}}/\text{cm}^{-1}$ 3073 (C-H aromatic), 2924 (CH_3 , CH_2), 2208 (CN), 1694 (CO), 1591 (C=C), 1427, 1302 (C-N, C-O). ^1H NMR

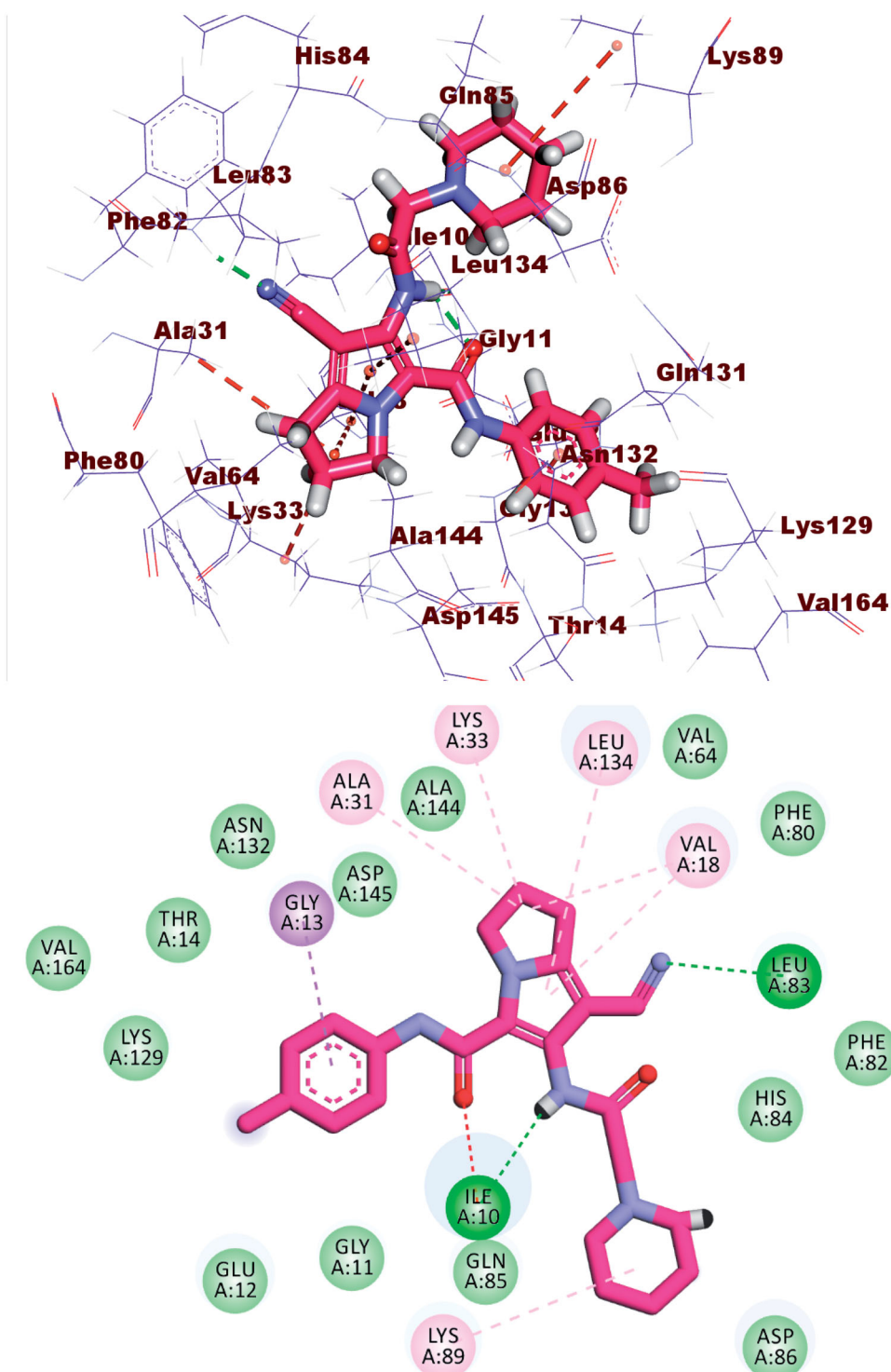


Figure 10. (A) Binding of compound 8b with CDK-2.

(CDCl₃, 400 MHz): δ 2.27 (s, 3H, CH₃C=N), 2.46 (s, 3H, CH₃Ph), 2.66 (m, 2H, CH₂-7), 3.18 (t, 2H, $J=7.6$ Hz, CH₂-8), 4.41 (t, 2H, $J=7.2$ Hz, CH₂-6), 7.12 and 7.37 (two d, 4H, $J=8$ Hz, *p*-substituted phenyl ring). ¹³C NMR (CDCl₃, 100 MHz): δ 21, 24.3, 25.1, 26.2, 48, 81.1, 113.5, 114, 127.9, 130.5, 137.2, 139.4, 148.5, 152.3, 154.1, 154.3. MS (EI): *m/z* (%) 305 (M⁺+1, 7), 304 (M⁺, 51), 122 (100). Anal. Calcd. for C₁₈H₁₆N₄O (304.35): C, 71.04; H, 5.30; N, 18.41. Found: C, 70.78; H, 5.50; N, 18.30.

4.1.6.3. 3-(4-Chlorophenyl)-2-methyl-4-oxo-4,6,7,8-tetrahydro-3H-pyrimido[4,5-b]pyrrolizine-9-carbonitrile (9c). The title compound was obtained from compound 5c as white crystals, m.p. 268–70 °C, yield 60%, IR_{max}/cm⁻¹ 3060 (C-H aromatic), 2924 (CH₃, CH₂), 2223 (CN), 1689 (CO), 1533 (C=C), 1419, 1300 (C-N, C-O), 840, 774 (C-Cl). ¹H NMR (CDCl₃, 400 MHz): δ 2.25 (s, 3H, CH₃C=N), 2.67 (m, 2H, CH₂-7), 3.19 (t, 2H, $J=7.2$ Hz, CH₂-8), 4.39 (t, 2H, $J=7$ Hz, CH₂-6), 7.19 and 7.54 (two d, 4H, $J=8$ Hz, *p*-substituted phenyl ring). ¹³C

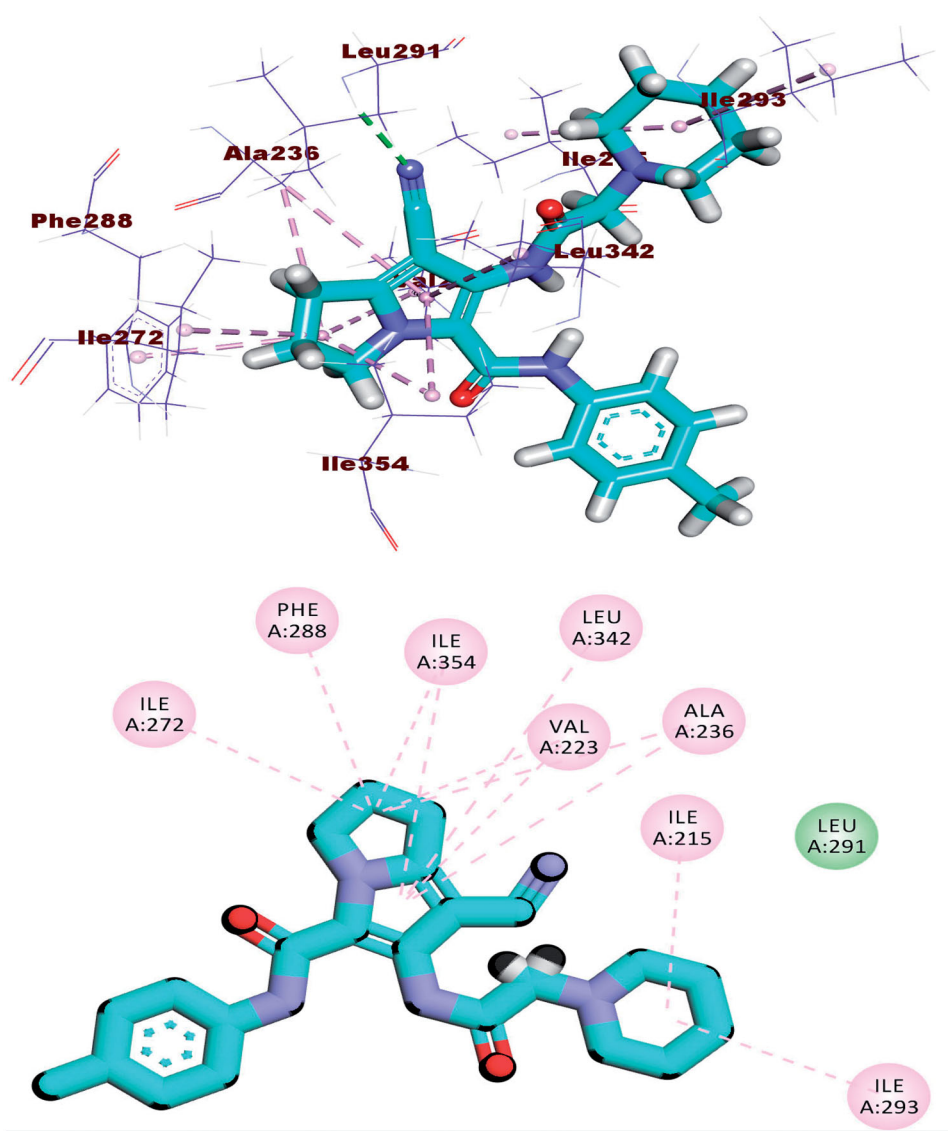


Figure 11. (A) Binding of compound 8b with DYRK3.

NMR (CDCl_3 , 100 MHz): δ 24.4, 25.2, 26.2, 48.1, 81.3, 113.3, 113.8, 129.5, 130.3, 135.6, 135.8, 148.4, 152.6, 153.7, 154.2. MS (EI): m/z (%) 324 (M^+ , 1), 91 (100). Anal. Calcd. for $\text{C}_{17}\text{H}_{13}\text{ClN}_4\text{O}$ (324.76): C, 62.87; H, 4.03; N, 17.25. Found: C, 62.69; H, 3.97; N, 17.55.

4.1.7. General method for preparation of compounds (11a-c)

To a solution of diazepino[5,6-*b*]pyrrolizine-10-carbonitrile derivative **10a-c** (3.26 mmol) in acetone, ethyl chloroacetate (0.4 g, 3.26 mmol) and anhydrous potassium carbonate (0.45 g, 3.26 mmol) was added. After refluxing for 6 h, the mixture was filtered and left to cool. The obtained white crystals were collected and recrystallized from ethanol.

4.1.7.1. Ethyl-2-(10-cyano-2,5-dioxo-4-phenyl-2,3,4,5,8,9-hexahydro-[1,4]diazepino[5,6-*b*]pyrrolizin-1(7H)-yl)acetate (11a). The title compound was obtained from compound **10a** as white crystals, m.p. 179–81 °C, yield 75%, $\text{IR}_{\text{max}}/\text{cm}^{-1}$ 3059 (C-H aromatic), 2977 (CH_2), 2220 (CN), 1740, 1693, 1643 (COs), 1549 (C=C), 1461, 1369, 1306 (C-N, C-O). ^1H NMR (CDCl_3 , 400 MHz): δ 1.29 (t, 3H, $J=7.2$ Hz, CH_3CH_2), 2.59 (m, 2H, CH_2 -8), 3.08 (t, 2H, $J=7.4$ Hz, CH_2 -9), 4.24 (q, 2H, $J=7.2$ Hz, CH_2CH_3), 4.39 (t, 2H, $J=7.2$ Hz, CH_2 -7), 4.49 (s, 2H,

CH_2 -3), 4.76 (s, 2H, NCH_2CO) and 7.29–7.46 (m, 5H, aromatic protons). ^{13}C NMR (CDCl_3 , 100 MHz): δ 14, 25.1, 25.4, 48.3, 49.3, 54.5, 61.9, 79.1, 114.2, 114.5, 125.7, 127.2, 129.2, 134.2, 141.6, 148.4, 159.6, 166.5, 167.5. MS (EI): m/z (%) 393 (M^+ , 1), 392 (M^+ , 1), 106 (100). Anal. Calcd. for $\text{C}_{21}\text{H}_{20}\text{N}_4\text{O}_4$ (392.41): C, 64.28; H, 5.14; N, 14.28. Found: C, 64.58; H, 5.36; N, 14.25.

4.1.7.2. Ethyl-2-(10-cyano-2,5-dioxo-4-(4-tolyl)-2,3,4,5,8,9-hexahydro-[1,4]diazepino[5,6-*b*]pyrrolizin-1(7H)-yl)acetate (11b). The title compound was obtained from compound **10b** as white crystals, m.p. 213–5 °C, yield 71%, $\text{IR}_{\text{max}}/\text{cm}^{-1}$ 3077 (C-H aromatic), 2970, 2924 (CH_3 , CH_2), 2220 (CN), 1741, 1690, 1642 (COs), 1548, 1465 (C=C), 1371, 1307 (C-N, C-O). ^1H NMR (CDCl_3 , 400 MHz): δ 1.28 (t, 3H, $J=7.2$ Hz, CH_3CH_2), 2.37 (s, 3H, CH_3Ph), 2.58 (m, 2H, CH_2 -8), 3.07 (t, 2H, $J=7.4$ Hz, CH_2 -9), 4.24 (q, 2H, $J=7.2$ Hz, CH_2CH_3), 4.40 (t, 2H, $J=7.2$ Hz, CH_2 -7), 4.46 (s, 2H, CH_2 -3), 4.75 (s, 2H, NCH_2CO), 7.21 and 7.30 (two d, 4H, $J=8.4$ Hz, *p*-substituted phenyl ring). ^{13}C NMR (CDCl_3 , 100 MHz): δ 14, 21, 25.1, 25.4, 48.3, 49.3, 54.6, 61.9, 79.1, 114.2, 114.6, 125.5, 129.8, 134.2, 137.2, 139, 148.2, 159.7, 166.5, 167.6. MS (EI): m/z (%) 407 (M^+ +1, 14), 406 (M^+ , 52), 186 (100). Anal. Calcd. for $\text{C}_{22}\text{H}_{22}\text{N}_4\text{O}_4$ (406.43): C, 65.01; H, 5.46; N, 13.78. Found: C, 65.30; H, 5.71; N, 13.77.

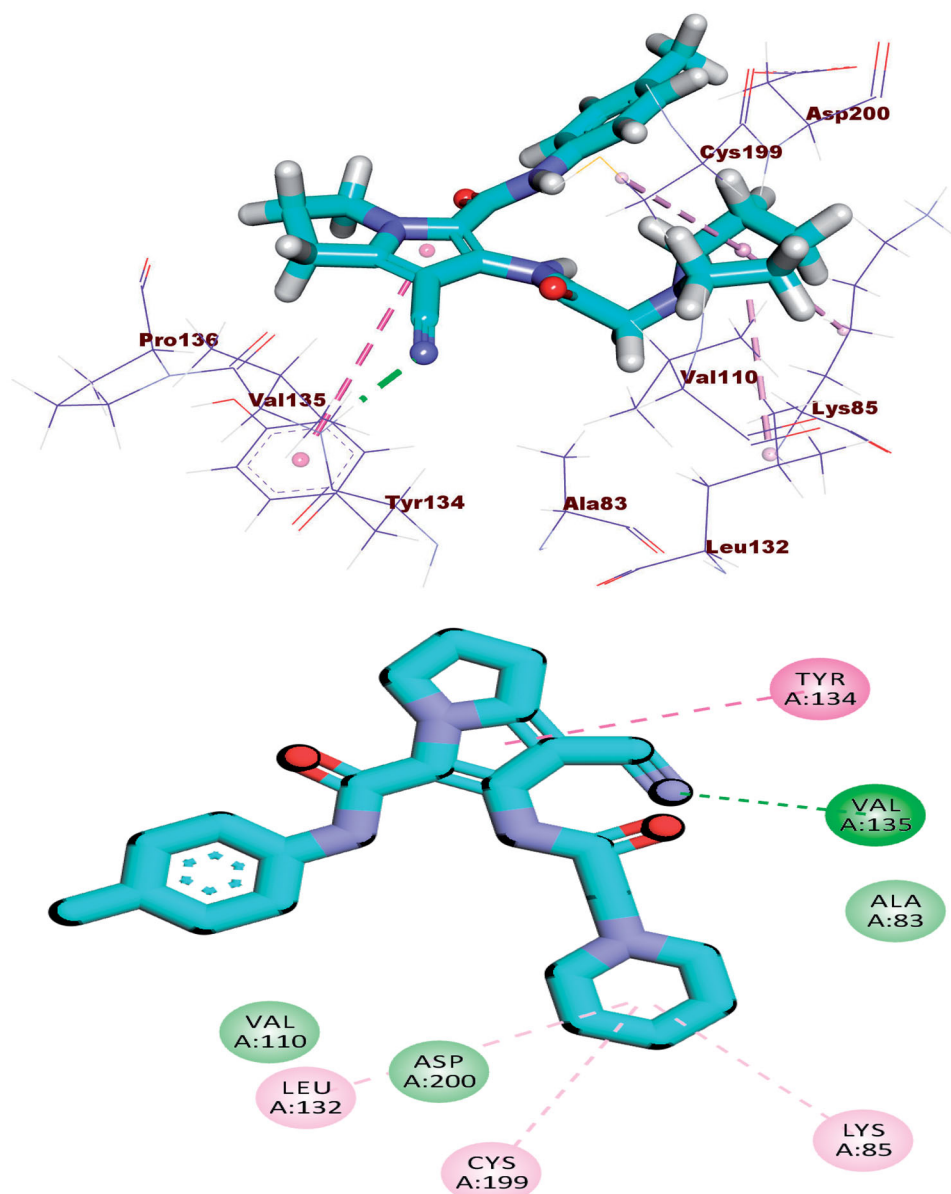


Figure 12. (A) Binding of compound 8b with GSK3 alpha.

Table 4. Toxicity properties of the synthesised compounds.

Comp.	FDA rodent carcinogenicity (mouse-female)	Carcinogenic potency TD ₅₀ (Rat) ^a	Rat maximum tolerated dose (feed) ^b	Rat oral LD ₅₀ ^b	Rat chronic LOAEL ^b	Ocular irritancy	Skin irritancy
6a	Single-Carcinogen	18.143	0.060	0.800	0.157	Irritant	Non-Irritant
6b	Non-Carcinogen	2.356	0.049	2.050	0.096	Irritant	Non-Irritant
6c	Non-Carcinogen	1.839	0.073	0.838	0.063	Irritant	Non-Irritant
8a	Non-Carcinogen	71.541	0.087	1.162	0.071	Irritant	Non-Irritant
8b	Non-Carcinogen	11.813	0.072	3.451	0.054	Irritant	Non-Irritant
8c	Non-Carcinogen	7.264	0.107	1.219	0.029	Irritant	Non-Irritant
9a	Non-Carcinogen	11.774	0.045	0.433	0.163	Irritant	Non-Irritant
9b	Non-Carcinogen	3.458	0.037	0.829	0.137	Irritant	Non-Irritant
9c	Non-Carcinogen	2.160	0.056	0.531	0.073	Irritant	Non-Irritant
11a	Non-Carcinogen	22.882	0.025	1.344	0.080	Irritant	Non-Irritant
11b	Non-Carcinogen	6.639	0.021	2.522	0.067	Irritant	Non-Irritant
11c	Non-Carcinogen	4.081	0.031	1.603	0.035	Irritant	Non-Irritant
Erlotinib	Non-Carcinogen	8.057	0.083	0.662	0.036	Irritant	Non-Irritant

^aUnit: mg/kg body weight/day.

^bUnit: g/kg body weight.

Table 5. Predicted ADMET profile for the synthesised compounds

Comp.	BBB level ^a	Solubility level ^b	Absorption level ^c	CYP2D6 prediction ^d	PPB prediction ^e
6a	4	2	1	False	True
6b	4	2	1	False	True
6c	4	2	2	False	True
8a	3	3	0	False	True
8b	3	2	0	False	True
8c	3	2	0	False	True
9a	2	2	0	False	True
9b	2	2	0	False	True
9c	2	2	0	False	True
11a	3	3	0	False	True
11b	3	3	0	False	True
11c	3	2	0	False	True
Erlotinib	1	2	0	False	True

^aBBB level, blood brain barrier level, 0 = very high, 1 = high, 2 = medium, 3 = low, 4 = very low.

^bSolubility level, 1 = very low, 2 = low, 3 = good, 4 = optimal.

^cAbsorption level, 0 = good, 1 = moderate, 2 = poor, 3 = very poor.

^dCYP2D6, cytochrome P2D6, TRUE = inhibitor, FALSE = non inhibitor.

^ePPB, plasma protein binding, FALSE means less than 90%, TRUE means more than 90%.

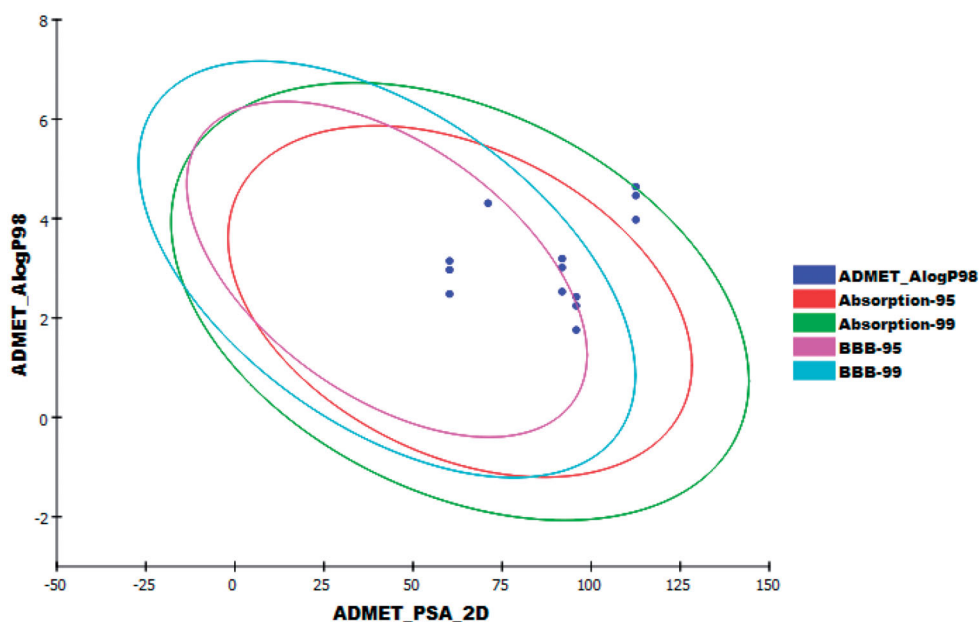


Figure 13. The expected ADMET study.

4.1.7.3. Ethyl-2-(4-(4-Chlorophenyl)-10-cyano-2,5-dioxo-2,3,4,5,8,9-hexahydro-[1,4]diazepino[5,6-b]pyrrolizin-1(7H)-yl)acetate (11c).

The title compound was obtained from compound **10c** as white crystals, m.p. 220–1 °C, yield 78%, IR_{max}/cm⁻¹ 3092 (C-H aromatic), 2970 (CH₂), 2222 (CN), 1749, 1686, 1647 (COs), 1549 (C=C), 1490, 1471, 1373, 1306 (C-N, C-O), 838, 772 (C-Cl). ¹H NMR (CDCl₃, 400 MHz): δ 1.28 (t, 3H, J = 7.2 Hz, CH₃CH₂), 2.60 (m, 2H, CH₂-8), 3.09 (t, 2H, J = 7.6 Hz, CH₂-9), 4.24 (q, 2H, J = 7.2 Hz, CH₂CH₃), 4.39 (t, 2H, J = 7.2 Hz, CH₂-7), 4.49 (s, 2H, CH₂-3), 4.75 (s, 2H, NCH₂CO), 7.38 and 7.43 (two d, 4H, J = 8.4 Hz, *p*-substituted phenyl ring). ¹³C NMR (CDCl₃, 100 MHz): δ 14.1, 25.2, 25.5, 48.4, 49.4, 54.4, 62, 79.3, 114.1, 114.4, 126.9, 129.4, 132.8, 134.4, 140, 148.6, 159.6, 166.4, 167.5. MS (EI): m/z (%) 428 (M⁺+2, 23), 426 (M⁺, 64), 186 (100). Anal. Calcd. for C₂₁H₁₉ClN₄O₄(426.85): C, 59.09; H, 4.49; N, 13.13. Found: C, 59.32; H, 4.39; N, 13.10.

4.2. Biological evaluation

4.2.1. In vitro anticancer screening

Cytotoxic activities evaluation of the synthesised compounds were done using the sulforhodamine B (SRB) method following the previous reported method⁶⁵ described in [Supplementary data](#).

4.2.2. Kinase profiling assay

Compound **8b** was selected to evaluate its inhibitory activity against 20 kinases according to the reported method.⁶⁶ The kinases inhibition assay was done by KINEXUS Corporation, Vancouver, BC, Canada, using the radiolabeled ATP determination method. Imatinib was used as a reference drug and blank control was set up and the corrected activity for the protein kinase target was determined. The results were presented as % inhibition, [Table 3](#).

4.2.3. Perturbation of cell cycle analysis

Cell cycle distribution analysis was performed for compounds **6a** and **8b** based on the previously described method in [Supplementary data](#)⁷⁷.

4.3. In silico studies

4.3.1. Docking studies

Crystallographic structures of EGFR CDK-2, and DYRK3, and GSK3 were retrieved from Protein Data Bank [PDB ID: 4HJO, resolution 2.75 Å and PDB ID: 6GUH, resolution 1.50 Å, PDB: 5Y86, resolution

1.90 Å, PDB: 5HLP, resolution 2.45 Å respectively] (<http://www.pdb.org>), and considered as targets for docking simulations. The docking analysis was performed using MOE software^{78–80} to evaluate the free energies and binding mode of the designed molecules against EGFR, CDK-2 and DYRK3, and GSK3. At first, the crystal structures of EGFR, CDK-2 and DYRK3, and GSK3 were prepared by removing water molecules and retaining only one chain and their co-crystallised ligands, erlotinib and AZD5438, HRM, and 65 A, respectively. Then, the protein structures were protonated, and the hydrogen atoms were hidden. Next, the energy was minimised, and the binding pockets of the protein were defined.

The 2D structures of the synthesised compounds and the co-crystallised ligands, erlotinib and AZD5438, HRM, and 65 A were sketched using ChemBioDraw Ultra 14.0 and saved as MDL-SD format. Then, the saved files were opened using MOE and 3D structures were protonated. Next, energy minimisation was applied. Before docking the synthesised compounds, validation of the docking protocol was carried out by running the simulation only using the co-crystallised ligands and low RMSD between docked and crystal conformations. The molecular docking of the synthesised compounds and the co-crystallised ligands was performed using a default protocol. MOE docking parameters include Triangle Matcher Algorithm with two rescoring functions London dG and GBVI/WSA dG were utilised to generate 10 poses of each compound. As a result, mdb output files were generated enclosing all docking results with scoring and multiple conformations of ligands. Results were finally inspected to determine the most promising compound by visualising various interactions of ligands within the binding pocket. The output from MOE was further analysed and visualised using Discovery Studio 4.0 software. The output from MOE was further analysed and visualised using Discovery Studio 4.0 software^{47,48,56,60}. Mutations, missing regions and active/inactive states of the receptors were presented in [Supplementary data](#).

4.3.2. In silico toxicity prediction

The toxicity parameters of the synthesised compounds were calculated using Discovery studio 4.0 as described in [Supplementary data](#)^{1,57}.

4.3.3. In silico ADMET studies

ADMET descriptors (absorption, distribution, metabolism, excretion, and toxicity) of the synthesised compounds were determined using Discovery studio 4.0 as described in [Supplementary data](#).

Disclosure statement

All authors of the above manuscript have not declared any conflict of interest.

Funding

Deanship of scientific research at Umm Al-Qura University supported this work by grant code (22UQU4290565DSR37).

ORCID

Amany Belal  <http://orcid.org/0000-0003-1045-0163>

Ahmed A. Al-Karmalawy  <http://orcid.org/0000-0002-8173-6073>

References

1. El-Metwally SA, Abou-El-Regal MM, Eissa IH, et al. Discovery of thieno [2, 3-d] pyrimidine-based derivatives as potent VEGFR-2 kinase inhibitors and anti-cancer agents. *Bioorg Chem* **2021**;112:104947.
2. World Health Organization, Cancer. Available from: <https://www.who.int/news-room/fact-sheets/detail/cancer> [last accessed 1 March 2020].
3. El-Zahabi MA, Sakr H, El-Adl K, et al. Design, synthesis, and biological evaluation of new challenging thalidomide analogs as potential anticancer immunomodulatory agents. *Bioorg Chem* **2020**;104:104218.
4. Chabner BA, Roberts TG. Chemotherapy and the war on cancer. *Nat Rev Cancer* **2005**;5:65–72.
5. G, Krauss N, Schönbrunner J, Cooper Biochemistry of signal transduction and regulation. Weinheim: Wiley Online Library; **2003**.
6. Nguyen K-SH, Kobayashi S, Costa DB. Acquired resistance to epidermal growth factor receptor tyrosine kinase inhibitors in non-small-cell lung cancers dependent on the epidermal growth factor receptor pathway. *Clin Lung Cancer* **2009**;10: 281–9.
7. Abbass EM, Khalil AK, Mohamed MM, et al. Design, efficient synthesis, docking studies, and anticancer evaluation of new quinoxalines as potential intercalative Topo II inhibitors and apoptosis inducers. *Bioorg Chem* **2020**;104:104255.
8. Al-Sanea MM, Elkamhawy A, Paik S, et al. Synthesis and biological evaluation of novel 3-(quinolin-4-ylamino) benzene-sulfonamides as carbonic anhydrase isoforms I and II inhibitors. *J Enzyme Inhib Med Chem* **2019**;34:1457–64.
9. Eldehna WM, Al-Rashood ST, Al-Warhi T, et al. Novel oxindole/benzofuran hybrids as potential dual CDK2/GSK-3 β inhibitors targeting breast cancer: design, synthesis, biological evaluation, and in silico studies. *J Enzyme Inhib Med Chem* **2021**;36:271–86.
10. Shaldam M, Eldehna WM, Nocentini A, et al. Development of novel benzofuran-based SLC-0111 analogs as selective cancer-associated carbonic anhydrase isoform IX inhibitors. *Eur J Med Chem* **2021**;216:113283.
11. Grant S. Therapeutic protein kinase inhibitors. *Cell. Mol. Life Sci* **2009**;66:1163–77.
12. Normanno N, De Luca A, Bianco C, et al. Epidermal growth factor receptor (EGFR) signaling in cancer. *Gene* **2006**;366: 2–16.
13. Sitohy B, Nagy JA, Dvorak HF. Anti-VEGF/VEGFR therapy for cancer: reassessing the target. *Cancer Res* **2012**;72:1909–14.
14. Touat M, Ileana E, Postel-Vinay S, et al. Targeting FGFR signaling in cancer. *Clin Cancer Res* **2015**;21:2684–94.
15. Morgan DO. Cyclin-dependent kinases: engines, clocks, and microprocessors. *Annu Rev Cell Dev Biol* **1997**;13:261–91.
16. Johnson LN, Noble ME, Owen DJ. Active and inactive protein kinases: structural basis for regulation. *Cell* **1996**;85:149–58.
17. Huang S-M, Harari PM. Epidermal growth factor receptor inhibition in cancer therapy: biology, rationale and preliminary clinical results. *Invest New Drugs* **1999**;17:259–69.
18. Salomon DS, Brandt R, Ciardiello F, Normanno N. Epidermal growth factor-related peptides and their receptors in human malignancies. *Crit Rev Oncol Hematol* **1995**;19:183–232.
19. Nicholson R, gee JM, harper M. egfR and cancer prognosis. *Eur J Cancer* **2001**;37:9–15.
20. Zhang H-Q, Gong F-H, Ye J-Q, et al. Design and discovery of 4-anilinoquinazoline-urea derivatives as dual TK inhibitors of EGFR and VEGFR-2. *Eur J Med Chem* **2017**;125:245–54.

21. Song Z, Huang S, Yu H, et al. Synthesis and biological evaluation of morpholine-substituted diphenylpyrimidine derivatives (Mor-DPPYs) as potent EGFR T790M inhibitors with improved activity toward the gefitinib-resistant non-small cell lung cancers (NSCLC). *Eur J Med Chem* **2017**;133:329–39.
22. Zhang Y, Chen L, Xu H, et al. 6, 7-Dimorpholinoalkoxy quinoxaline derivatives as potent EGFR inhibitors with enhanced antiproliferative activities against tumor cells. *Eur J Med Chem* **2018**;147:77–89.
23. Belal A. Synthesis, molecular docking and antitumor activity of novel pyrrolizines with potential as EGFR-TK inhibitors. *Bioorg Chem* **2015**;59:124–9.
24. Jaiash DA, Belal A, Abdelgawad MA, Abdellatif KR. Design, synthesis and biological evaluation of new pyrroloazepines with potential and selective antitumor activity. *Acta Poloniae Pharmaceutica* **2016**;73:359–68.
25. Ding L, Cao J, Lin W, et al. The roles of cyclin-dependent kinases in cell-cycle progression and therapeutic strategies in human breast cancer. *Int J Mol Sci* **2020**;21:1960.
26. Belal A. 3D-pharmacophore modeling, molecular docking, and virtual screening for discovery of novel CDK4/6 selective inhibitors. *Russian J Bioorg Chem* **2021**;47:317–33.
27. Asghar U, Witkiewicz AK, Turner NC, Knudsen ES. The history and future of targeting cyclin-dependent kinases in cancer therapy. *Nat Rev Drug Discov* **2015**;14:130–46.
28. Ahn YM, Vogeti L, Liu C-J, et al. Design, synthesis, and antiproliferative and CDK2-cyclin a inhibitory activity of novel flavopiridol analogues. *Bioorg Med Chem* **2007**;15:702–13.
29. Peng C, Zeng W, Su J, et al. Cyclin-dependent kinase 2 (CDK2) is a key mediator for EGF-induced cell transformation mediated through the ELK4/c-Fos signaling pathway. *Oncogene* **2016**;35:1170–9.
30. Yang A-I, Wu Q, Hu Z-d, et al. A network pharmacology approach to investigate the anticancer mechanism of cinobufagin against hepatocellular carcinoma via downregulation of EGFR-CDK2 signaling. *Toxicol Appl Pharmacol* **2021**;431:115739.
31. Joshi A, Bhojwani H, Wagal O, et al. Evaluation of benzamide-chalcone derivatives as EGFR/CDK2 inhibitor: synthesis, in-vitro inhibition, and molecular modeling studies, anti-cancer agents in medicinal chemistry (formerly current). *Anti-cancer Agents Med Chem* **2022**;22:328–43.
32. Mediani L, Antoniani F, Galli V, et al. Hsp90-mediated regulation of DYRK3 couples stress granule disassembly and growth via mTORC1 signaling. *EMBO Reports* **2021**;22:e51740.
33. Wippich F, Bodenmiller B, Trajkovska MG, et al. Dual specificity kinase DYRK3 couples stress granule condensation/dissolution to mTORC1 signaling. *Cell* **2013**;152:791–805.
34. Papadopoli D, Pollak M, Topisirovic I. The role of GSK3 in metabolic pathway perturbations in cancer. *Biochim Biophys Acta (BBA)-Mol Cell Res* **2021**;1868:119059.
35. Quintayo MA, Munro AF, Thomas J, et al. GSK3 β and cyclin D1 expression predicts outcome in early breast cancer patients. *Breast Cancer Res Treat* **2012**;136:161–8.
36. Patel P, Woodgett JR. Glycogen synthase kinase 3: a kinase for all pathways? *Curr Top Dev Biol* **2017**;123:277–302.
37. Bonomi P. Erlotinib: a new therapeutic approach for non-small cell lung cancer. *Expert Opin Investig Drugs* **2003**;12:1395–401.
38. Ou S-HI. Second-generation irreversible epidermal growth factor receptor (EGFR) tyrosine kinase inhibitors (TKIs): a better mousetrap? A review of the clinical evidence. *Crit Rev Oncol Hematol* **2012**;83:407–21.
39. Walter AO, Sjin RTT, Haringsma HJ, et al. Discovery of a mutant-selective covalent inhibitor of EGFR that overcomes T790M-mediated resistance in NSCLC. *Cancer Discovery* **2013**;3:1404–15.
40. Sequist LV, Besse B, Lynch TJ, et al. Neratinib, an irreversible pan-ErbB receptor tyrosine kinase inhibitor: results of a phase II trial in patients with advanced non-small-cell lung cancer. *J Clin Oncol* **2010**;28:3076–83.
41. Kim Y, Ko J, Cui Z, et al. The EGFR T790M mutation in acquired resistance to an irreversible second-generation EGFR inhibitor. *Mol Cancer Therap* **2012**;11:784–91.
42. Zhao Z, Wu H, Wang L, et al. Exploration of type II binding mode: a privileged approach for kinase inhibitor focused drug discovery? *ACS Chem Biol* **2014**;9:1230–41.
43. Furet P, Caravatti G, Lydon N, et al. Modelling study of protein kinase inhibitors: binding mode of staurosporine and origin of the selectivity of CGP 52411. *J Comput Aided Mol Des* **1995**;9:465–72.
44. Gandin V, Ferrarese A, Dalla Via M, et al. Targeting kinases with anilinoimidazoles: discovery of N-phenyl-N'-[4-(pyrimidin-4-ylamino) phenyl] urea derivatives as selective inhibitors of class III receptor tyrosine kinase subfamily. *Sci Rep* **2015**;5:16750.
45. Liu Y, Gray NS. Rational design of inhibitors that bind to inactive kinase conformations. *Nat Chem Biol* **2006**;2:358–64.
46. Zhang J, Yang PL, Gray NS. Targeting cancer with small molecule kinase inhibitors. *Nat Rev Cancer* **2009**;9:28–39.
47. Elmetwally SA, Saied KF, Eissa IH, Elkhaed EB. Design, synthesis and anticancer evaluation of thieno [2, 3-d] pyrimidine derivatives as dual EGFR/HER2 inhibitors and apoptosis inducers. *Bioorg Chem* **2019**;88:102944.
48. Nasser AA, Eissa IH, Oun MR, et al. Discovery of new pyrimidine-5-carbonitrile derivatives as anticancer agents targeting EGFR WT and EGFR T790M. *Org Biomol Chem* **2020**;18:7608–34.
49. Traxler P, Furet P. Strategies toward the design of novel and selective protein tyrosine kinase inhibitors. *Pharmacol Therap* **1999**;82:195–206.
50. Malki Y, Martinez J, Masurier N. 1, 3-Diazepine: a privileged scaffold in medicinal chemistry. *Med Res Rev* **2021**;41:2247–315.
51. Xu T, Zhang L, Xu S, et al. Pyrimido [4, 5-d] pyrimidin-4 (1H)-one derivatives as selective inhibitors of EGFR threonine790 to methionine790 (T790M) mutants. *Angewandte Chemie* **2013**;125:8545–8.
52. Ibrahim M, Taghour M, Metwaly A, et al. Design, synthesis, molecular modeling and anti-proliferative evaluation of novel quinoxaline derivatives as potential DNA intercalators and topoisomerase II inhibitors. *Eur J Med Chem* **2018**;155:117–34.
53. Mahdy HA, Ibrahim MK, Metwaly AM, et al. Design, synthesis, molecular modeling, in vivo studies and anticancer evaluation of quinazolin-4 (3H)-one derivatives as potential VEGFR-2 inhibitors and apoptosis inducers. *Bioorg Chem* **2020**;94:103422.
54. El-Naggar AM, Eissa IH, Belal A, El-Sayed AA. Design, eco-friendly synthesis, molecular modeling and anticancer evaluation of thiazol-5 (4H)-ones as potential tubulin polymerization inhibitors targeting the colchicine binding site. *RSC Adv* **2020**;10:2791–811.

55. Eissa IH, Metwaly AM, Belal A, et al. Discovery and antiproliferative evaluation of new quinoxalines as potential DNA intercalators and topoisomerase II inhibitors. *Archiv Der Pharmazie* **2019**;352:1900123.
56. Eissa IH, Ibrahim MK, Metwaly AM, et al. Design, molecular docking, in vitro, and in vivo studies of new quinazolin-4 (3H)-ones as VEGFR-2 inhibitors with potential activity against hepatocellular carcinoma. *Bioorg Chem* **2021**;107:104532.
57. Alanazi MM, Eissa IH, Alsaif NA, et al. Design, synthesis, docking, ADMET studies, and anticancer evaluation of new 3-methylquinoxaline derivatives as VEGFR-2 inhibitors and apoptosis inducers. *J Enzyme Inhib Med Chem* **2021**;36:1760–82.
58. Hagra M, El Deeb MA, Elzahabi HS, et al. Discovery of new quinolines as potent colchicine binding site inhibitors: design, synthesis, docking studies, and anti-proliferative evaluation. *J Enzyme Inhib Med Chem* **2021**;36:640–58.
59. Alanazi MM, Elwan A, Alsaif NA, et al. Discovery of new 3-methylquinoxalines as potential anti-cancer agents and apoptosis inducers targeting VEGFR-2: design, synthesis, and in silico studies. *J Enzyme Inhib Med Chem* **2021**;36:1732–50.
60. Gaber AA, Bayoumi AH, El-Morsy AM, et al. Design, synthesis and anticancer evaluation of 1H-pyrazolo [3, 4-d] pyrimidine derivatives as potent EGFRWT and EGFR790M inhibitors and apoptosis inducers. *Bioorg Chem* **2018**;80:375–95.
61. El-Moghazy SM, Hanna MM, Farag AE, Belal A. Synthesis and biological evaluation of some novel substituted pyrrolizines and pyrimidopyrrolizines as Chemotherapeutic agents. *Der Chemica Sinica* **2017**;8(1):102–16.
62. Shaaban HG. Synthesis of some heterocyclic compounds derived from 2-chloro-Np-tolylacetamide. *Al-Mustansiriyah J Sci* **2017**;27. DOI:10.23851/mjs.v27i4.26
63. Gouda AM, Abdelazeem AH, Arafa E-SA, Abdellatif KR. Design, synthesis and pharmacological evaluation of novel pyrrolizine derivatives as potential anticancer agents. *Bioorg Chem* **2014**;53:1–7.
64. Khademi Z, Nikoofar K. Applications of alkyl orthoesters as valuable substrates in organic transformations, focusing on reaction media. *RSC Adv* **2020**;10:30314–97.
65. Skehan P, Storeng R, Scudiero D, et al. New colorimetric cytotoxicity assay for anticancer-drug screening. *JNCI: J Natl Cancer Inst* **1990**;82:1107–12.
66. Elsayed MS, El-Araby ME, Serya RA, et al. Structure-based design and synthesis of novel pseudosaccharine derivatives as antiproliferative agents and kinase inhibitors. *Eur J Med Chem* **2013**;61:122–31.
67. El-Helby A-GA, Ayyad RR, El-Adl K, Elkady H. Phthalazine-1, 4-dione derivatives as non-competitive AMPA receptor antagonists: design, synthesis, anticonvulsant evaluation, ADMET profile and molecular docking. *Mol Divers* **2019**;23:283–98.
68. El-Helby AGA, Ayyad RR, Zayed MF, et al. Design, synthesis, in silico ADMET profile and GABA-A docking of novel phthalazines as potent anticonvulsants. *Archiv Der Pharmazie* **2019**;352:1800387.
69. Abdallah AE, Alesawy MS, Eissa SI, et al. Design and synthesis of new 4-(2-nitrophenoxy) benzamide derivatives as potential antiviral agents: molecular modeling and in vitro antiviral screening. *N J Chem* **2021**;45:16557–71.
70. Xia X, Maliski EG, Gallant P, Rogers D. Classification of kinase inhibitors using a Bayesian model. *J Med Chem* **2004**;47:4463–70.
71. BIOVIA, QSAR, ADMET and predictive toxicology. <https://www.3dsbiovia.com/products/collaborative-science/biovia-discovery-studio/qsar-admet-and-predictive-toxicology.html> [last accessed May 2020].
72. Alanazi MM, Elkady H, Alsaif NA, et al. Discovery of new quinoxaline-based derivatives as anticancer agents and potent VEGFR-2 inhibitors: design, synthesis, and in silico study. *J Mol Struct* **2022**;1253:132220.
73. Alsaif NA, Taghour MS, Alanazi MM, et al. Discovery of new VEGFR-2 inhibitors based on bis ([1, 2, 4] triazolo)[4, 3-a: 3', 4'-c] quinoxaline derivatives as anticancer agents and apoptosis inducers. *J Enzyme Inhib Med Chem* **2021**;36:1093–114.
74. Alanazi MM, Elkady H, Alsaif NA, et al. New quinoxaline-based VEGFR-2 inhibitors: design, synthesis, and antiproliferative evaluation with in silico docking, ADMET, toxicity, and DFT studies. *RSC Adv* **2021**;11:30315–28.
75. Alsaif NA, Dahab MA, Alanazi MM, et al. New quinoxaline derivatives as VEGFR-2 inhibitors with anticancer and apoptotic activity: design, molecular modeling, and synthesis. *Bioorg Chem* **2021**;110:104807.
76. Abbas SE, Awadallah FM, Ibrahim NA, et al. Design, synthesis and preliminary evaluation of some novel [1, 4] diazepino [5, 6-b] pyrrolizine and 6-(2-oxopyrrolidino)-1H-pyrrolizine derivatives as anticonvulsant agents. *Med. Chem. Res* **2011**;20:1015–23.
77. Nicoletti I, Migliorati G, Pagliacci M, et al. A rapid and simple method for measuring thymocyte apoptosis by propidium iodide staining and flow cytometry. *J Immunol Methods* **1991**;139:271–9.
78. Hammouda MM, Abo Elmaaty A, Nafie MS, et al. Design and synthesis of novel benzoazoninone derivatives as potential CBSIs and apoptotic inducers: In Vitro, in Vivo, molecular docking, molecular dynamics, and SAR studies. *Bioorg Chem* **2022**;127:105995.
79. Belal A, Elanany MA, Santali EY, et al. Screening a panel of topical ophthalmic medications against MMP-2 and MMP-9 to investigate their potential in keratoconus management. *Molecules* **2022**;27:3584.
80. Chemical Computing Group, Molecular Operating Environment (MOE). <http://www.chemcomp.com/> [last accessed May 2017].